

MECHANICAL PROPERTIES OF POLYMER-CLAY NANOCOMPOSITE THIN
FILMS

by

Sarah Hutcheson, B.S.

A thesis submitted to the Graduate Council of
Texas State University in partial fulfillment
of the requirements for the degree of
Master of Science
with a Major in Chemistry
December 2021

Committee Members:

Gary W. Beall, Chair

L. Kevin Lewis

Maedeh Dabbaghianamiri

COPYRIGHT

by

Sarah Hutcheson

2021

FAIR USE AND AUTHOR'S PERMISSION STATEMENT

Fair Use

This work is protected by the Copyright Laws of the United States (Public Law 94-553, section 107). Consistent with fair use as defined in the Copyright Laws, brief quotations from this material are allowed with proper acknowledgement. Use of this material for financial gain without the author's express written permission is not allowed.

Duplication Permission

As the copyright holder of this work I, Sarah Hutcheson, refuse permission to copy in excess of the "Fair Use" exemption without my written permission.

ACKNOWLEDGEMENTS

I would like to express my deep and sincere gratitude for my advisor, Dr. Gary Beall for all the patience and mentoring he has provided throughout all stages of this work. I am truly humbled by his guidance. This would not have been possible without him.

I would also like to thank my committee members, Dr. Dabbaghianamiri and Dr. Lewis for their expertise, encouragement, and thoughtful comments and suggestions along the way.

I would also like to acknowledge with great appreciation my mentors, colleagues, friends, and family for their continuous support and understanding throughout my research.

TABLE OF CONTENTS

	Page
ACKNOWLEDGEMENTS	iv
LIST OF TABLES	vii
LIST OF FIGURES	viii
LIST OF ABBREVIATIONS.....	xi
ABSTRACT.....	xii
CHAPTER	
1. INTRODUCTION	1
1.1 Industry Motivation.....	1
1.2 Mineral Clay Molecular Structure.....	2
2. SMECTITE CLAY NANOPARTICLES	4
2.1 Ionic Clay Characterization.....	4
2.2 Montmorillonite.....	4
2.3 Laponite.....	8
2.4 Functionalization.....	9
3. PROPERTIES OF CLAY NANOCOMPOSITES	23
3.1 Thermodynamics	23
3.2 Mechanical Properties	30
3.3 Thermal Properties	36
3.4 Barrier Materials.....	37
3.5 Optical Properties	45

4. POLY(VINYL ALCOHOL)/MONTMORILLONITE NANOCOMPOSITE THIN FILMS.....	48
4.1 Introduction.....	48
4.2 Experimental.....	50
4.3 Data and Analysis.....	56
4.4 Conclusions.....	60
REFERENCES	62

LIST OF TABLES

Table	Page
1. Selected chemical and physical properties of comparative clay species	6
2. Basic parameters of LAP	8
3. PCN preparation by weight in DI water	51
4. PCN species and thin film applications parameters.....	52
5. PCN tensile values as compared to neat PET	59

LIST OF FIGURES

Figure	Page
1. A representation of (a) silicon tetrahedron, and (b) aluminum octahedron	2
2. A representation of the structural layers of clays.....	3
3. Schematic representation of the final structure corresponding to sheet 2:1	4
4. FTIR spectrum of pure MMT	6
5. Comparative XRD patterns of Na-MMT and Fe-MMT	7
6. Crystal structure of LAP.....	8
7. Effect of hydration time on dispersibility of LAP	9
8. Imaging of morphology and microstructure of exfoliated MMT (a) TEM, (b) AFM ...	11
9. XRD pattern of neat vs. cationic surfactant modified MMT	12
10. Reaction scheme of aminosilane and nanosilicate.....	13
11. Storage modulus of pure HDPE and HDP/ silane-modified clays	14
12. Thermographs of pure clay, polymer, and their polymer obtained via solution method (a) and melt blending (b).....	16
13. Scheme thin film deposition via dip coating method.....	18
14. Principles of dip, spin, and spray coating deposition methods	19
15. Topography of printing drop structures of different sizes dried at 60C on PET substrate (a, b, c) and cross sectional profiles of dried drop structures of the composite inks (n=256)	21
16. Cross sectional ion beam etched SEM images of printed drops after drying	22
17. Composite morphologies of polymer-clay constituent dispersions	23

18. SEM cross section of MMT film before (a) and after (b) exfoliation and evaporation (scale bar: 2 μ m)	25
19. FTIR spectra of MMT-H ₂ O mixtures in the 400 < $\Delta\omega$ < 4000 cm ⁻¹ spectral range vs. time	25
20. Interfacial tension of PS-clay systems at room temperature.....	28
21. Influence of thermodynamic work of adhesion at room temperature on the modulus of nanocomposites (a) PS1510 and (b) PS1220 prepared with organoclays at two concentrations of clays.....	29
22. Tensile testing of MMT/PVA nanocomposites as a function of MMT content	32
23. Stress-strain curve of MMT/PVA composites as a function of MMT weight and volume fraction	33
24. SEM images of MMT/PVA cross sections at 10% (a), 30% (b), 50% (c), and 70% (d).....	34
25. Strength comparisons of intercalated vs. exfoliated nanoclay composites.....	34
26. RVE damage distribution in nanoclay composites	35
27. Thermal stability of organo-modified clays.....	36
28. Schematic of Hofmann elimination as onium salt degradation produces an olefin, an amine, and a counterion on organo-modified clays	37
29. $\Delta\%$ weight of composites with varying MMT content in solutions	38
30. Bode impedance plots from GA-crosslinked PCN-coated steel coupons in bilayers applications of (a) 20, (b) 40, and (c) 60 over 168 hours. Bar graph (d) shows low frequency impedance (0.1 Hz) value for each thickness over time	39
31. Tortuous Path model of clay platelets in polymer nanocomposites	40
32. (a) OTR and permeability as a function of PVAm-based quadlayers deposited on PET and (b) as a function of quadlayer recipe and number of depositions	42
33. Heat shielding abilities of clay films exposed to flame at different distances and temperatures over time.....	43
34. Conceptualization of air voids in fundamental units of multilayered structures of NSP and MMT films	44
35. Peak heat release rates for polystyrene polymer and three nanocomposites	45

36. Structural scheme of original versus hydrothermally treated clay particles and their behaviors	46
37. Reflectance intensity of PCN coating on copper plates (a) and measured reflectance relate to bare copper (b) via UV-VIS spectroscopy	47
38. Hydrolysis reaction mechanism yielding polyvinyl alcohol.....	48
39. Chemical structure of polyvinyl alcohol.....	49
40. UV-VIS absorption spectra of S0 (neat PVA film), S1 (120°C, 80 min), S2 (140°C, 75 min), S3 (160°C, 70 min), S4 (180°C, 30 min), S5 (180°C, 65 min).....	50
41. Fujifilm Dimatix DM-2831 inkjet printer and cartridges	52
42. Dimatix print cartridge nozzle sizes as compared to a quarter	53
43. PCN film during printing, showing discrete droplets at non-uniform sizes	54
44. Clay before (in solution) and after (in syringe) filtration to demonstrate color change	54
45. Mechanical tensile testing equipment used for thin films deposited on PET substrate	55
46. Neat PET Stress-Strain curve.....	56
47. Stress-Strain curves of PCN applications of PCN in various combinations.....	57
48. Stress-strain curves of solitary clay or polymer coatings as compared to neat PET ...	59
49. Microscope imagining of PVOH 0.3 / MMT 0.45 at 24 layers at 5x, 10x and 20x resolution.....	60
50. Microscope imagining of Premix PVOH 0.3 / MMT 0.45 at 12 layers at 5x, 10x, 20x resolution.....	60
51. Microscope imagining of PVP 0.3/LAP 0.45 at 24 layers 5x, 10x, 20x resolution.....	60

LIST OF ABBREVIATIONS

Abbreviation	Description
MMT, Na-MMT	Na ⁺ montmorillonite [(Na)(Al ₂)(Si ₄ O ₁₀)(OH) ₂]
PCN	Polymer Clay Nanocomposite
PVOH or PVA	Poly(vinyl alcohol) [(C ₂ H ₄ O) _n]
LAP	Laponite [(Na _{0.7})[(Si ₈ Mg _{5.5} Li _{0.3})O ₂₀ (OH) ₄]
HEC	Hectorite [(Na _{0.3} (Mg,Li) ₃ Si ₄ O ₁₀ (OH) ₂]
DI	Deionized Water
PVP	Polyvinylpyrrolidone [(C ₆ H ₉ NO) _n]
CEC	Cation Exchange Capacity (meq/100g)
LBL	Layer-by-layer
PET	Polyethylene terephthalate [(C ₁₀ H ₈ O ₄) _n]
T _g	Glass transition temperature
CTE	Coefficient of thermal expansion
TMA	Thermomechanical analysis
XRF	X-ray fluorescence
TGA	Thermogravimetric analysis
E	Young's Modulus
Pa	Pascal (N/m ²)
XRD	X-ray diffraction

ABSTRACT

Clay-containing polymer nanocomposites applied as thin films have been found to have superior mechanical properties over isolated clay or polymer treatments. The majority of early studies of polymer-clay nanocomposites (PCNs), contain only 2 to 5% of clay relative to polymer and become very brittle when the concentration exceeds 10%. Studies in our lab have discovered self-assembling PCNs that contain as much as 50% clay yet retains flexibility. This thesis reports on the physical properties of these self-assembling PCNs. The composition and concentration of polymers and clays chosen for this work is inherently non-toxic, inexpensive, and ideal as a packaging additives. PCNs were prepared with water-soluble vinyl polymers and cationic phyllosilicate clays in low combinatory concentrations in the dispersed phase (>1% by weight) and applied to substrate as layered thin film coatings. PCN films with ductile polymers maintained flexibility, transparency, and mechanical performance. Tensile strength of the PCN coated substrate were shown to increase as a result of layer-by-layer (LBL) spray coating treatments, even at loadings as low as 0.3% and film thicknesses of 0.01 mm.

Neat PET substrate treated with clay solutions of 0.45% LAP or MMT increased tensile strength by 106% and 158% with 12 layers of applications and total coating thicknesses of 0.01 and 0.02 mm, respectively. The same trend was observed for PVOH and PVP polymer coatings solutions of 0.3%.

‘Premixed’ polymer/clay solutions outperformed neat substrate, solitary clays and polymer films but not films of alternating polymer/clay layers of the same concentration

Combinatory bilayered polymer/clay treatments of PET in either 12 or 24 layers showed an increase in tensile strength from that of layered treatments of only clays or polymers with coating thicknesses ranging from 0.03 to 0.05 mm.

PVP 0.3% and LAP 0.45% at 24 layers (12 bilayers) at a total film thickness of 0.05 mm increased tensile strength of substrate by 475% and increased yield and failure points considerably. Construction of bilayered LAP and PVP appeared to be more cohesive than adhesive to substrate, allowing deformation at the film before fracturing at substrate and increasing mechanical strength.

Durability and chemical resistance appeared to improve for PCNs as a function of treatment, assembly, and evaporation on the substrate, making the thin films practical as protective barriers. Optical transparency and flexibility and were maintained for PCNs with the exception of MMT, which may be modified with proper purification processing.

PCNs prepared with synthetic vinyl polymers prepared in combination with phyllosilicate clays display self-assembly behavior and intercalation interactions ideal for application as reinforcement and performance materials. When applied layer-by-layer via spray coating deposition, PCNs produced thin film coatings with increased tensile strength at relatively low loadings making them highly applicable as environmentally friendly packaging alternatives.

1. INTRODUCTION

1.1 Industry Motivation

With increasing awareness of anthropogenic activity and the reduction of petroleum resources, the production of biodegradable plastic materials derived from natural and renewable resources is gaining traction in both academia and industry [26]. The flexible packaging industry reported \$33.6 billion in sales in the US in 2019 and global consumer demand is projected to continue increasing substantially [1]. Recently, functionalized nanocomposites have attracted significant interest due to their low cost, high performance, and exceptional mechanical properties even when applied as thin film coatings. Polymer composites containing 2D layered nanosheet clays as reinforcing fillers are an ideal combination to produce physical, chemical, and gas resistant protective barriers [2]. Platelet layered clays have large surface areas, high aspect ratios, and cationic exchange capabilities that make them highly desirable as composite additives. Additionally, PCNs with attractive thermoplastic behavior such as those synthesized with ionic clays and hydrophilic polymers have been shown to increase mechanical strength and stability for targeted applications. Due to inherent interlayer interactions, intelligent PCN design parameters result in self-assembled nanostructures with tunable physiochemical properties such as surface charge and hydrophobicity. PCNs synthesized with biodegradable, nontoxic clays and water-soluble polymers could prove to be a safe, inexpensive, and low effluence solution for sustainable, environmentally friendly practices. Despite new efforts to employ similar techniques, the packaging industry often fails to offer feasible low-waste substitutions as evidenced by the EPA estimated 14.5

million tons of plastic containers and packaging generated in 2018 [3]. However, thin film depositions of PCNs could provide novel opportunities as flexible, durable, and transparent protective coatings for consumers and suppliers as an alternative packaging solution.

1.2 Mineral Clay Molecular Structure

Clay minerals are known as phyllosilicates and have a basic silicon-oxygen (Si-O) tetrahedron whereby one silicon cation (Si^{4-}) is surrounded by four oxygen anions (O^{-2}). Layered sheet silicates have planar structures and are defined by SiO_4 tetrahedral layers (Figure 1a) coordinated with divalent or trivalent cations of octahedral layers (Figure 1b) [4].

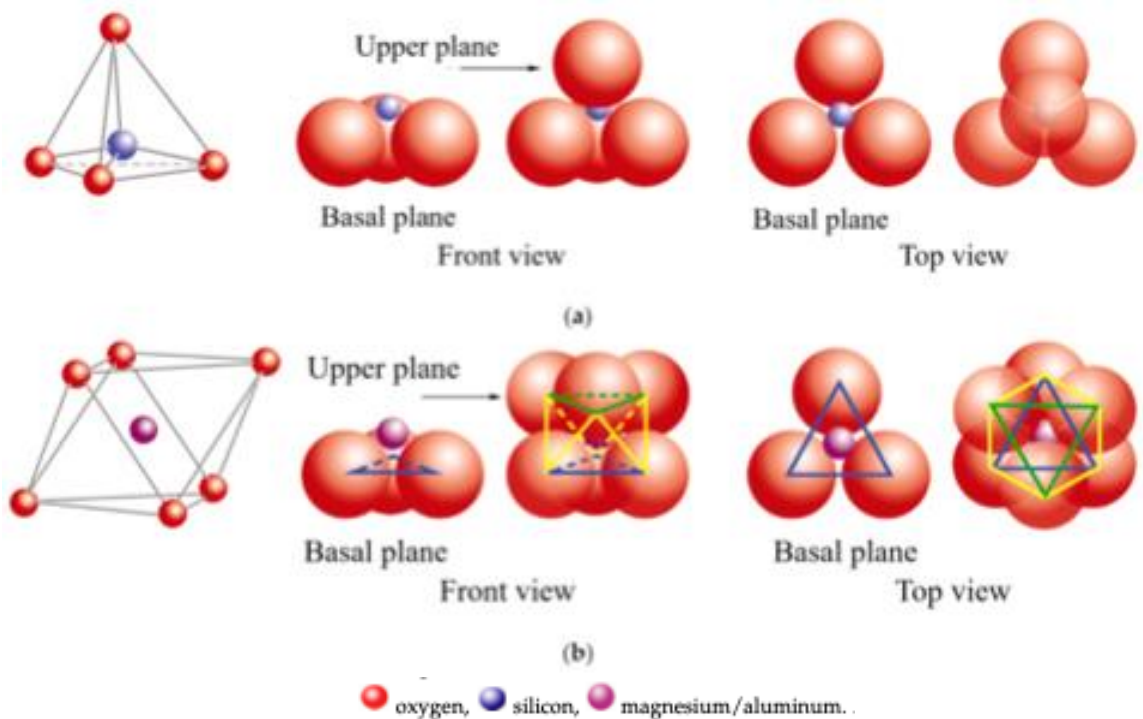


Figure 1: A representation of (a) silicon tetrahedron, (b) magnesium and / or aluminum octahedron

In this permutation, the octahedral layers share oxygen and hydroxyl anion groups at edges that form the two-dimensional hexagonal patterns. The arrangement of tetrahedral (Figure 2a) and octahedral layers (Figure 2b) through atomic planes constitutes the fundamental unit of various sheet clay's structure [4]. Due to polymorphic properties of clay, families of minerals are defined by the configuration of the unit structure of the alternating sheet stacking patterns of the parallel planes.

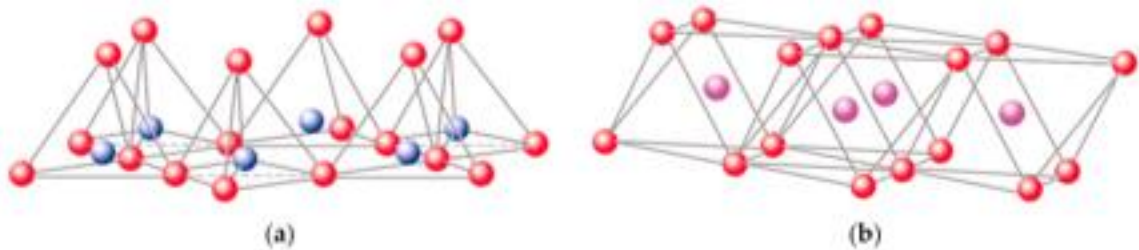


Figure 2: A representation of structural layers of clays: (a) silicon tetrahedron (b) magnesium and / or aluminum octahedron

Functionalization of advantageous structural properties of clay minerals has been utilized in many fields such as water remediation and pharmaceuticals as well as additives for applications including protective coatings such as flame retardants, gas barriers, sealants and reflectives. As the technology sector has increased, the rise in development of modified clay nanocomposites with clays with tunable physical and chemical properties for subsequent surface treatments.

2. SMECTITE CLAY NANOPARTICLES

2.1 Ionic Clay Characterization

Lamellar solids of clay minerals are categorized by the charge of the layers and the ionic species that compensate for charge imbalances within interlayer regions of the clay [13]. Cationic clays such as naturally occurring, ubiquitous montmorillonite (MMT) and synthetic laponite (LAP) have negatively charged layers.

2.2 Montmorillonite

Smectic clays are classified as having a layered mesomorphic state in which the axis of molecules is perpendicular to the plane of distinct 2:1 tetrahedral and octahedral layers arranged as platelet sheets. One such naturally occurring smectic clay, montmorillonite (MMT: $[(Al_2)(Si_4O_{10})(OH)_2Na_x \cdot nH_2O]$) is a dioctahedral aluminosilicate belonging to the 2:1 classification of clay minerals. The fundamental structure of MMT is composed of a single cationic metal oxide octahedral center layer inserted between two layers of silicon tetrahedral structures stacked in parallel planes with hexagonal symmetries (Figure 3).

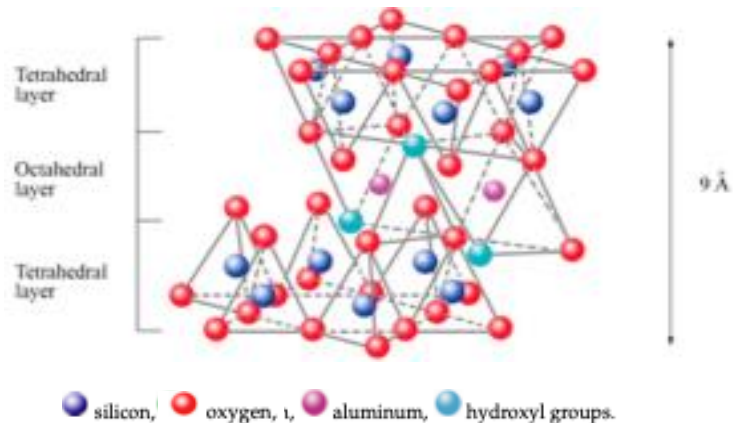


Figure 3: Schematic representation of the final structure corresponding to sheet 2:1

Octahedral basal oxygen atoms linked to metal oxides form the union between layers of different geometries and the charge balance produces hydroxyl groups (OH) of the center planes. The dioctahedral cation, (Al^{3+}) thus maintains the structural arrangements within unit configurations via intermolecular interactions. MMT is turbostratic which means that the individual plates are not crystallographically related. This can be seen in the x-ray diffraction pattern where only $hk0$ and $00l$ reflections can be observed with total absence of hkl reflections.

The interlaminar space between two consecutive 2:1 sheet units are known as “galleries” and contain exchangeable cations. This interlayer spacing within galleries is thereby able to expand or contract as divalent metal species which undergo isomorphic substitution of the silicate crystal structure. The resultant charge imbalance is overcome by exchangeable cations on the surface and is formally characterized as the cation exchange capacity (CEC) of the clay. The edge-shared octahedra sheets of MMT are coordinated by oxygen and cationic hydroxyls (Al^{3+}) capable of ion substitution with lower valent species (Na^+ , K^+ , Ca^{2+} , Mg^{2+}) [4]. Swelling behavior of MMT is in large part due to cation compensation and variable surface charges as a result of substitution activity at tetrahedral and octahedral sites (Al^{3+} , Si^{4+} respectively) [5].

The FTIR spectrum of pure MMT as shown in Figure 4 is characterized by two major bands. The vibrational bands at 3697 cm^{-1} and 3623 cm^{-1} attributed to OH groups coordinated with octahedral ions whereby the 3623 cm^{-1} band indicates substitution of the Al^{3+} cations [10]. The OH stretching band in the frequency range of $2700\text{-}3900\text{ cm}^{-1}$ is dependent on the hydration within the MMT matrix.

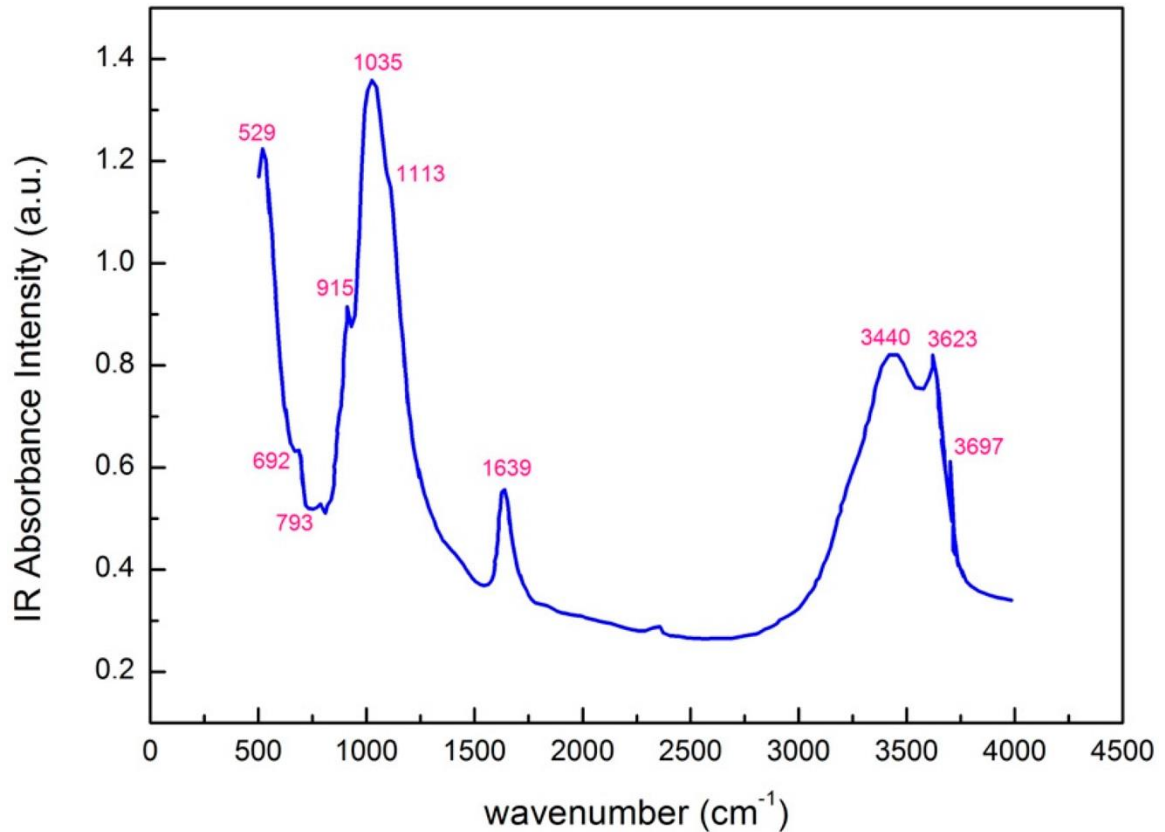


Figure 4: FTIR spectrum of pure MMT 14 [10]

Most uncontaminated phyllosilicates present extensive swelling capacities with d_{001} values of basal spacing in MMT ranging from 0.95 to 1.9 nm as interlayers expand when interacting with water molecules in the interstitial space [2]. Relative physical and chemical properties of comparable clay species (Table 1) reflects the delineation of MMT's CEC, hydration capacity and high surface area.

Table 1: Selected chemical and physical properties of comparative clay species [11]

Property	Kaolinite	Illite	Montmorillonite
Tactoid size (μm) ^a	0.1-5.0	0.2-2.0	0.01-1.0
Layer charge (x) ^b	<0.01	1.4-2	0.5-1.2
Cation exchange capacity ($\text{meq } 100^{-1}$) ^c	2	27	76
Specific surface area ($\text{m}^2 \text{g}^{-1}$) ^d	24	95	750-780
Hydration at 105 °C (%) ^e	1	4	7

^a Tactoid size determined by AFM.

^b Data from Sposito et al., 1999. x = moles of excess charge per chemical formula unit.

^c Data from source Source Clays Repository and Ward's Science.

^d Specific surface area determined by EGME.

^e Hydration at 105 °C determined by thermal gravimetric analysis.

Given the weak nature of intermolecular attraction and platelet morphology, the lamellar units of individual MMT crystals are not tightly bound and therefore allow for water intervention. Additionally, functionally treated MMT species such as Na⁺-exchanged MMT (Na-MMT) has further increased preferential adsorption energy and CEC due to its monovalent nature and relatively small atomic radius, allowing for intercalation of larger, polar, and organic molecular structures in the interstitial gallery space. Ion exchange can effectively thereby increase the d₀₀₁ value of MMT as Na⁺ cations (0.095nm) are replaced with Fe³⁺ (0.064nm). The basal spacing is seen shifting from a d₀₀₁ value of 1.55nm for pristine Na-MMT to 1.34nm for Fe-MMT as displayed by X-ray diffraction (XRD) patterns in Figure 5 [12].

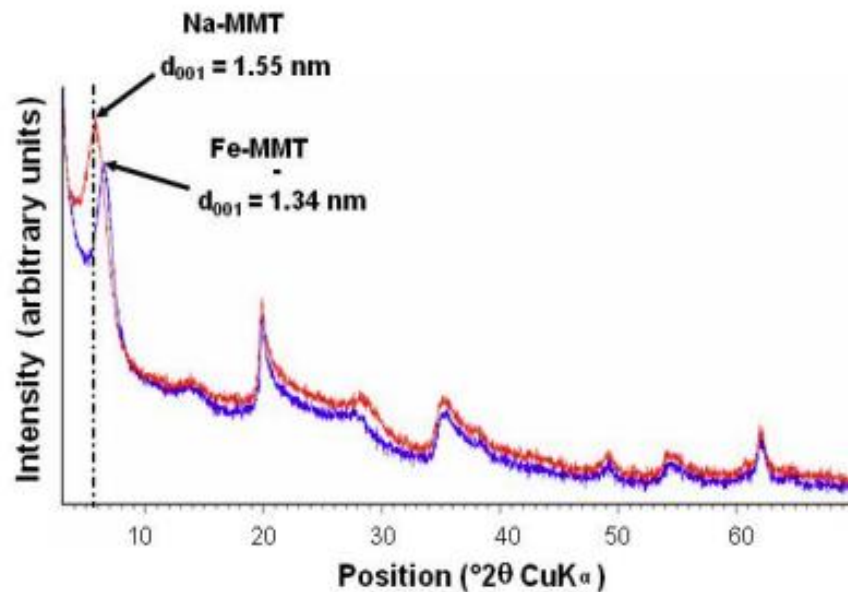


Figure 5: Comparative XRD patterns of Na-MMT and Fe-MMT

The swelling behavior of MMT is an integral phenomenon owing to its ubiquitous use in a wide array of industrial applications.

2.3 Laponite

Laponite (LAP) is a synthetic smectite clay with a structure and composition closely resembling the natural clay mineral hectorite (HEC: $\text{Na}_{0.3}(\text{Mg},\text{Li})_3\text{Si}_4\text{O}_{10}(\text{OH})_2$) [22]. HEC is a trioctahedral 2:1 layer silicate with MgO interlayer (Figure 6) [24].

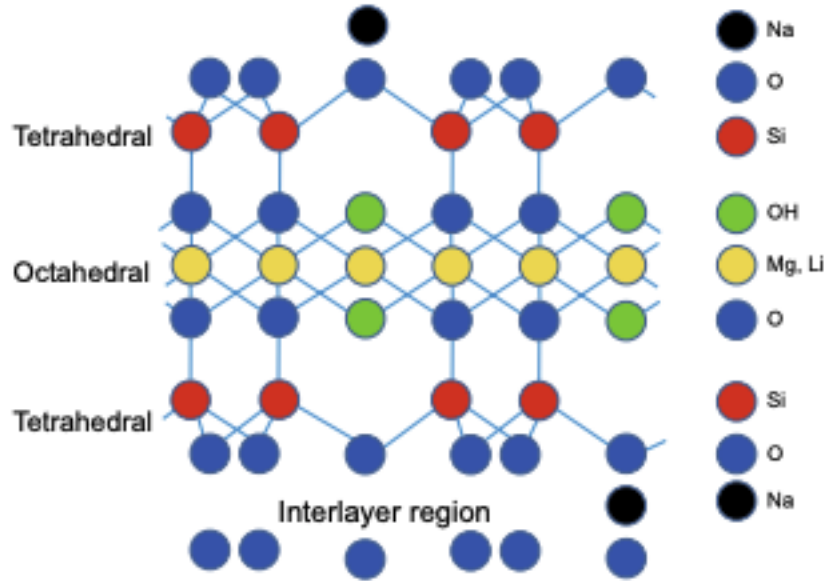


Figure 6: Crystal structure of LAP

However, HEC clay is scarce in nature and often contains many complex impurities that are difficult to remove [23]. The high-purity, synthetic form of HEC, LAP presents similar properties as MMT clay: superior CEC, interlayer cations (typically Na^+ and Li^+), dispersibility in water and additional parameters as stated in Table 2.

Table 2: Basic parameters of LAP

Bulk density, g/cm^3	Surface area (BET), m^2/g	pH (2 wt% aqueous suspension)	Cation exchange capacity, $\text{meq}/100 \text{ g}$
0.7–1.3	300–400	9.8	50–60

Due to its excellent heat resistance and additive compatibility, commercial LAP has been successfully utilized as a rheological modifier as thickening or thixotropic agent in many coatings and personal care products. When added to distilled water at low weight concentrations (0.5-4%), dispersibility of LAP is indicated as apparent viscosity values where full hydration of dosages <1% steadily rise and remain steady at ~6-8 hours (Figure 7).

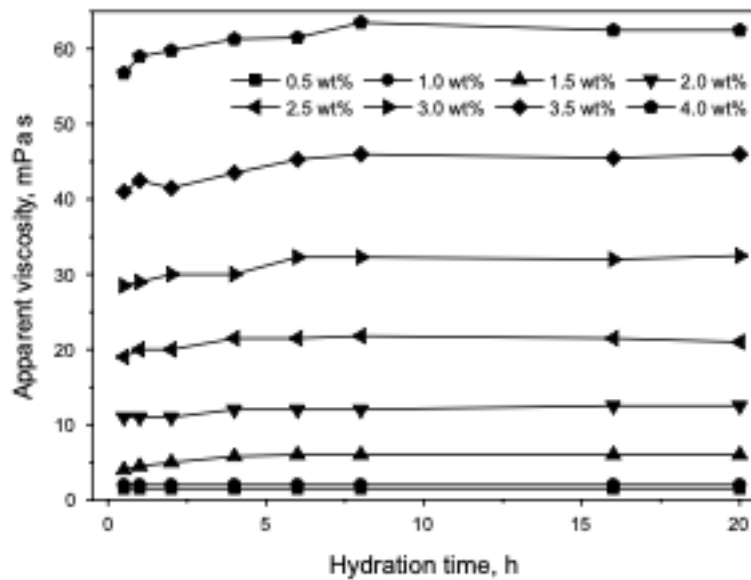


Figure 7: Effect of hydration time on dispersibility of LAP

2.4 Functionalization

Inorganic layered silicates such as MMT is the most commonly used nanoreinforcement material used by the plastic industry as an additive for improved flame retardancy, mechanical and barrier properties [28]. Mineral MMT particles possess advantageous aggregate behaviors such as the ability to direct polymer species into dispersed-phase galleries during self-assembly of PCNs. Functional modifications of clay

minerals morphological structures (also referred to as organomodification or organofoliation) control the degree of intercalation or exfoliation of silicate layers and influence the distribution and reinforcement of nanofillers within the layers. Polymer-clay nanocomposites (PCNs) are a class of composites constituted as having a silicate-based poly-dispersed phases of particles with at least one dimension in the nanometer range (10^{-9} m). Colloidal behavior and performance of plate-like clay structures in PCNs are largely dependent on the surface area to volume ratios. Exfoliated MMT particles produce nanoplatelets about 1nm thick with an aspect ratio of 100-500 and surface areas of 700-800m²/g [7] and make for excellent fillers in functionalized PCNs.

2.4.1 Treatment

Advantageous properties of ionic clays such as CEC and swelling capability make for excellent sorbent materials for selectively permeable membranes in applications like water filtration, desalination, and molecular sieves. However, the same rich nanochannels that allow for functionalization can also cause attraction and retention of impurities within galleries. Raw clay minerals, whether synthetic or natural may require purification of containments before further processing. Prescence of organic impurities can pose challenging to remove in aqueous systems once swelling occurs from oxygen-containing functional groups bound within interlayers. General purification can be performed at the site of extraction and includes grinding in water to form a slurry which is then filtered or re-diluted and subsequently precipitated. However, more aggressive contamination may require further chemical or mechanical separation in order to maximize functionality of nanocomposite constituents for optimal utility.

Performance and stability of nanocomposites is contingent on control of the degree of separation and structural reformation of individual nanoparticles and distribution of clay within polymer matrices during polymerization. Effective liquid-phase exfoliation of commercially available Na-MMT can be carried out by vigorous mixing in DI water, ultrasonication, centrifugation, and vacuum filtration [29]. The resultant MMT nanosheets produced from this procedure are thin and nearly transparent, as seen in the TEM image (Figure 8a) and presented thickness ~ 1.8 nm (Figure 8b), suggesting a qualitative majority product of monolayered nanosheets.

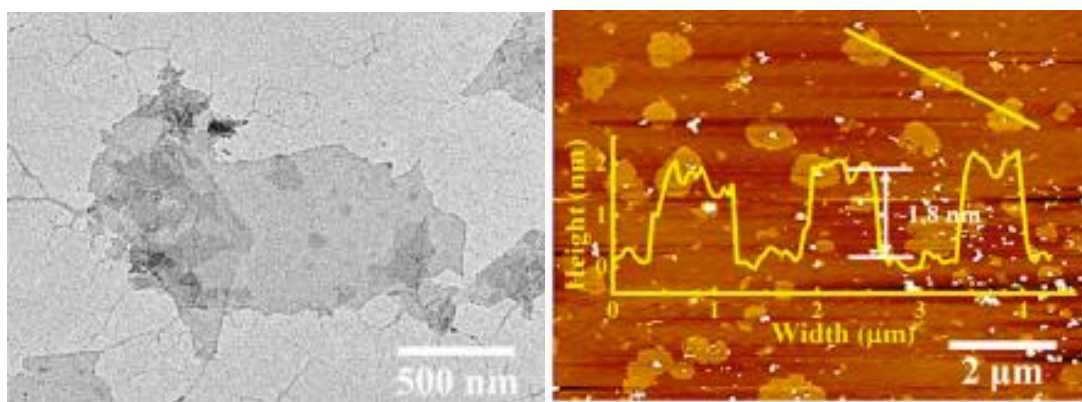


Figure 8: Imaging of morphology and microstructure of exfoliated MMT (a) TEM, (b) AFM

2.4.2 Surface modification

In addition to prerequisite treatment and characterization, surface treatment has been shown to improve compatibility or alter bonding sites with polymer matrices [30]. Synthesis of PCNs with unmodified, ionic clays can cause agglomeration in the polymer matrix due to their intrinsic hydrophilicity [30]. Surface modification of nanoclays has been proven to increase mechanical properties of PCN production [34]. A conventional modification method involves ion exchange via intercalation of organic surfactants between clay layers. Cationic surfactant loading with quaternary alkylammonium

compounds has been shown to increase the basal spacing by methodically tuning the surface affinity for hydration [31]. The intergallery distance $d(001)$ is dependent on the alkyl chain length and confirmed with XRD patterns of neat versus surfactant-modified MMT (Figure 9) whereby basal spacing is seen increasing from 1.21 nm to 2.0 nm respectively [31].

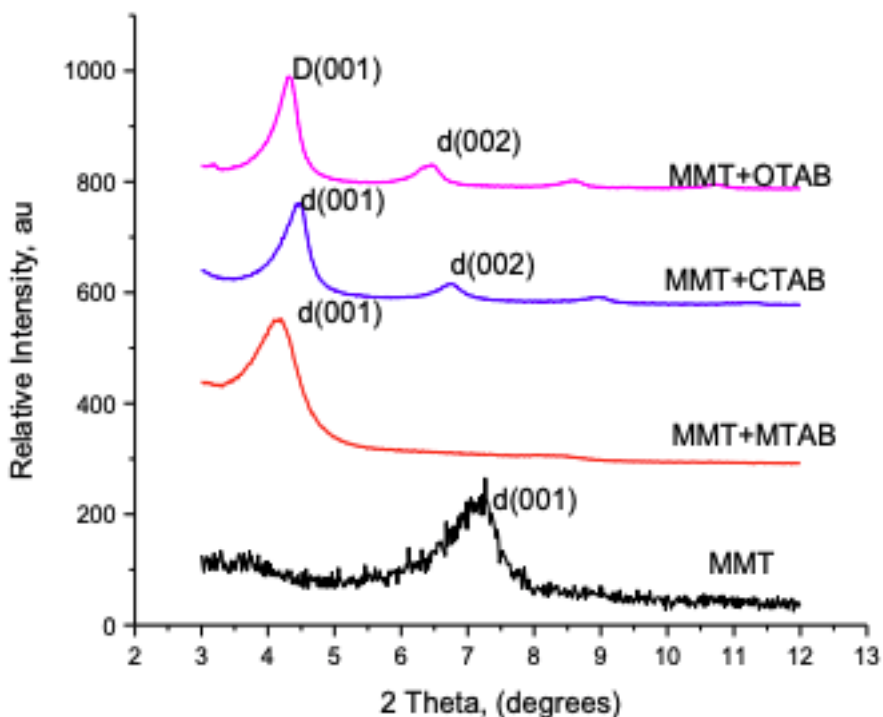


Figure 9: XRD pattern of neat vs. cationic surfactant modified MMT

Ion exchange surface modification by silane treatment has also been shown to improve the functionalized intercalation of MMT and dispersibility in polymer media [31]. Chemical grafting of silane coupling agents improves the adhesion of vinyl ester resins to alumina within clay galleries [32] and silane-modified clays outperformed pure HDPE polymer in rheological properties and tensile modulus [33]. The proposed

mechanism of aminosilane molecules reaction with nanosilicates is presented in Figure 10.

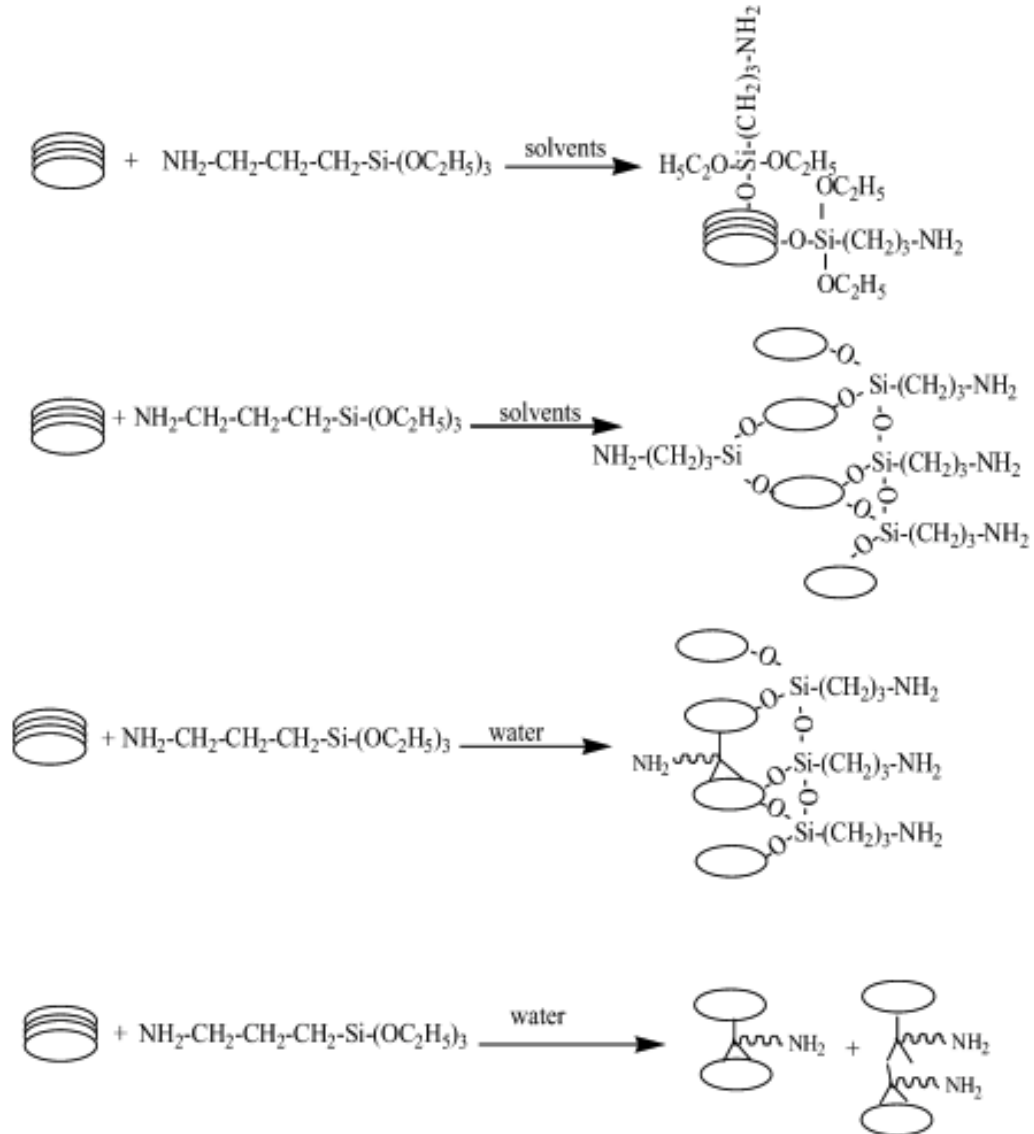


Figure 10: Reaction scheme of aminosilane and nanosilicate

As available hydroxyl groups interact with silane, $d(001)$ values increase as interlayer spaces are penetrated by alkoxy silane molecules. Addition of solvents was employed to chemically graft silanes between platelets however, the degree of salinization was dependent on the surface energy of the solvent systems with regard to

the polarity of the clay. A condensation reaction is proposed as non-hydrolyzed segments of silane coupling agents form Si-O-Si bonds at the scaffolding basal spacing by bridging concurrent platelets. Interlocking networks are thereby formed between and at the platelet edges. When added in excess, steric hindrance of higher concentrations of silane molecules further restrict silane movement and incorporation [33].

MMT treated with γ -aminopropyltriethoxysilane (γ -APTES) has been shown to improve dispersion in an HDPE nanocomposite [33]. Additionally, Untreated Na-MMT and silane-modified Na-MMT incorporated into HDPE show significant mechanical property differences as shown in Figure 11.

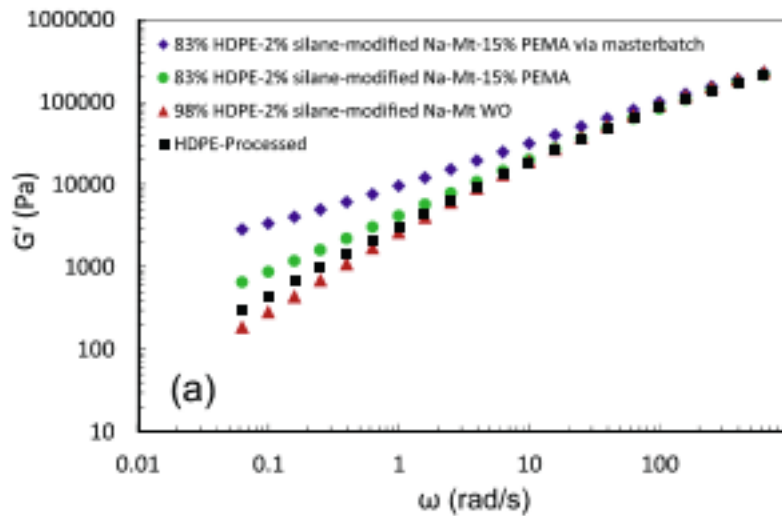


Figure 11: Storage modulus of pure HDPE and HDP/ silane-modified clays

2.4.3 Synthesis and polymerization

Nanocomposites refer to multiphase materials where at least one of the constituent phases has one dimension less than 100 nm [27]. Advantages of nanocomposites can be achieved even at low clay load ratios due to the high aspect ratio of the particles, dispersibility, and attraction of bulk polymer within interlayers. During in

situ technique, clay particles are dispersed into a monomer-containing solvent and the solution is polymerized, often in the presence of initiators or catalysts. Homogeneous PVOH-hybrid composites have been synthesized from polymer precursors and simultaneous hydrolysis of functional groups via simple acidic catalysts [35]. There exists a myriad of developments in incorporation techniques for preparing PCNs. Due in part to their simplicity, among the most favorable in-situ polymerization techniques are melt mixing and solution method.

2.4.3.1 Solution method

The solution method is particularly suitable for preparation of PCNs with water soluble polymers which disperse at relatively low temperatures. Clay-polyethyleneterephthalate (PET) PCNs were prepared using a solution technique of organic solvent mixture and ultrasonication. The procedure yielded composites where complete exfoliation of clay layers into the polymeric matrix was achieved with dimethyl dioctadecyl ammonium modified MMT as evidenced by no significant clay diffraction peak during XRD studies, as compared to pristine MMT at $2\theta = 5.5^\circ$ (15.9 \AA) [36].

In one modified solution method experiment, a solution of ethylene vinyl acetate, and p-xylene were mixed at 80°C for 5 hours before addition of organoclay and a temperature ramp of 180°C and constant stirring for an additional 35 hours produced dispersions with exfoliated morphology. The dispersions are supposed as resulting from mobility of molecular chains of polymers which permits penetration of the gallery space of the clay particles at room temperature followed by solvent evaporation and PCN formation at an increased temperature [37].

2.4.3.2 Melt blending

Melt mixing is a common technique for composite thermoplastic production and can be easily applied to synthesis of PCNs. Melt mixing can be carried out without the addition of solvents or polymer monomers, making it attractive for industrial and batch production.

Although modified solution method has proven efficient for obtaining PCNs with exfoliated morphology of silicate layers, melt blending of comparative species has been shown to produce composites with better thermal stability and melting behavior (Figure 12) [37].

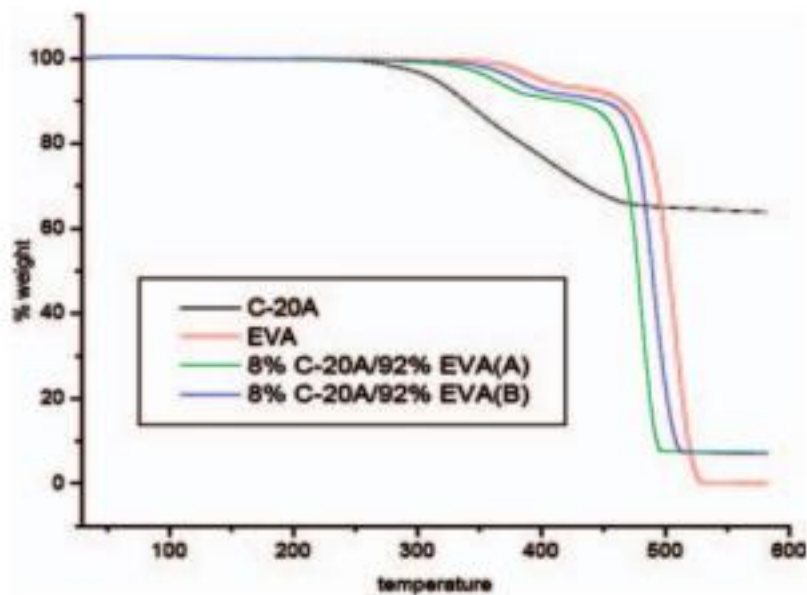


Figure 12: Thermographs of pure clay, polymer, and their polymer obtained via solution method (a) and melt blending (b)

Additionally, melt blended PCNs outperform solution method yields in mechanical stress testing and gas and vapor permeability and is considered a characteristic due to superior exfoliation and dispersion quality [38].

2.4.4 Thin Film Deposition Methodologies

High performance PCN coatings require controlled deposition of functionalized surfaces and multifunctional protective barriers. Utilizing layer-by-layer (LBL) technique produces multilayered, ultrathin films with maximum coverage of water dispersible polymers and clay nanoparticles. PCNs deposited as thin films on a substrate via LBL can be implemented in several manners: alternating inorganic/organic bilayers, multilayering independent, sequential applications of inorganics/organics in progressive pattern, or multiple applications of PCN slurry solutions. Alternating deposition of compatible inorganic/organic or, clay/polymer layers results in self-assembly of highly ordered composite films during application whereas slurry mixtures self-assemble in-situ and harden at evaporation. Homogeneity in treatment of compounding layers is achievable in scalable applications due to the inherent self-assembly properties and high surface area of PCNs with platelet structures. Accounting for preservation of PCN functionality, several excellent alternatives to mechanical coating of LBL applications are presented.

2.4.4.1 Dip Coating

A more conventional LBL process of thin film fabrication, dip coating is a relatively straight forward technique where substrate is immersed directly into coating solution. Dip coating technique consists of film coating onto substrate surface when withdrawn from waterborne suspensions of PCN solutions and is usually performed at room temperature (Figure 13).

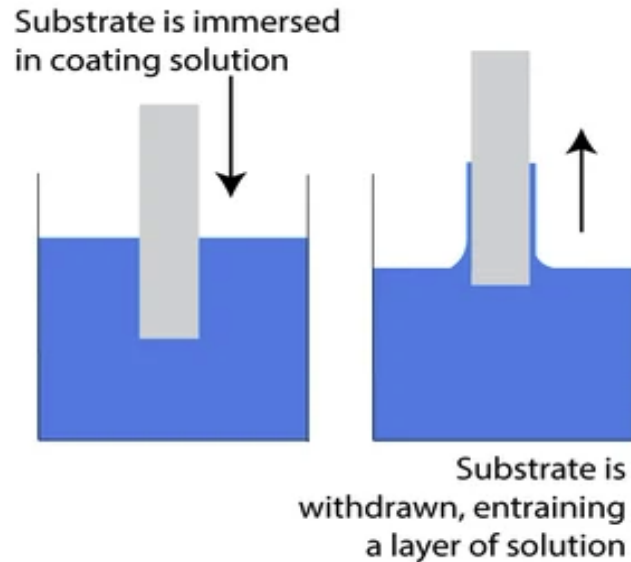


Figure 13: Scheme thin film deposition via dip coating method

Dip coating allows for reproducible deposition control of film thickness by speed and angle regulation during withdraw from solution. However, dip coating relies on multiple cycles of substrate immersion, rinsing and drying [39]. Although LBL dip coating can achieve great uniformity and high precision batch processing, this technique poses challenges to implement on a commercial scale due to time, space, and wastewater constraints required for progressive cycles [40]. One significant drawbacks of this technique is the limitations of particulate geometry homogeneity. Coating solutions with high aspect ratio or highly viscosity such as PCN solutions with platelet morphologies can cause gravitational flow in solution during withdraw, causing edge defects, and aggregation of particles that increase dry time and impact uniformity.

2.4.4.2. Spin coating

Spin coating is commonly used commercially in electronics industry for deposition of silicon wafers [58]. This technique utilizes centrifugal force for spreading coating solution upon a rotating substrate. Much like dip coating, spin coating is highly

reproducible and requires simple automation methods. Compared to dip coating which requires a solution bath, spin coating requires significantly less solution to cover substrate although, solution not adhered to substrate during spin coating is considered wasted and cannot be reclaimed for bulk solution.

Despite precision realized in spin coating, any micro or macro deformations in substrate cause surface defects that are compounded in LBL applications due to minute changes in flow rate and angular velocity. Similar to downfalls of dip coating, fluid dynamics such as particle dimensions and surface tension properties of PCN solution constituents can affect homogeneity during spin coating applications.

2.4.4.3 Spray coating

Spray coating is an excellent option for quick and efficient coating application of thin films. Spray coating method employs atomization of PCN solution whereby film formation occurs at suspension droplet impact on substrate. Layer deposition is controlled by the parameters: drop size, pressure, distance, and angle at the aperture of the spray nozzle [57]. This method is highly versatile and can be easily integrated for non-planar surfaces [59]. Despite adaptability of spray coating, reproducibility of uniform layers is highly dependent on the operator and scale-up requires meticulous parameter control.

Figure 14 summarizes the principles of the deposition methods mentioned thus far [57].

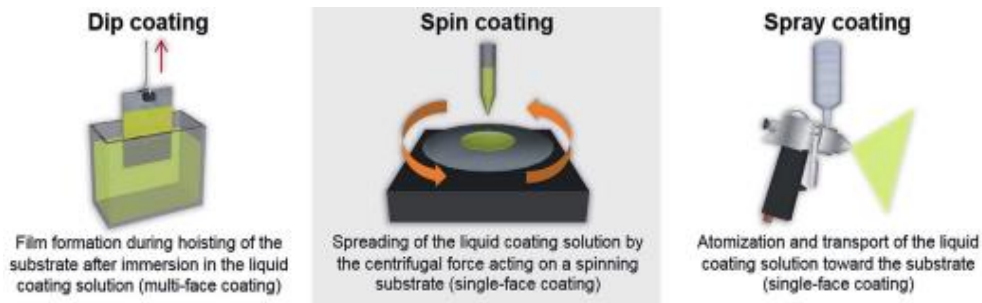


Figure 14: Principles of dip, spin, and spray coating deposition methods

2.4.4.4 Doctor Blading

Doctor blading, also known as knife or blade coating is a thin film fabrication method that involves constant distribution over substrate. As solution is moved over substrate a fraction is deposited through the gap between blade and substrate and the excess removed by the blunt blade edge, controlling film thickness throughout the blade diameter.

2.4.4.5 Inkjet Printing

Industrial development and use of commercial inkjet printers have proved beneficial for direct fabrication from design, without the need for patterning or masks. Recent research has demonstrated innovative alternative techniques that advantageously utilize inherent self-assembly qualities of PCNs. Drop on Demand (DOD) inkjet printing is one such contactless alternative as it does not require lengthy intermediate steps and produces enhanced homogeneity due to excellent parameter control during application. Composite formulation for inkjet printing requires consideration of particle size, surface tension and viscosity as it relates to the dimensions of the printhead nozzles [41]. Printable material must also be compatible to media surface for adherence.

Ceramic/polymer composite inkjet formulations of $\text{Ba}_{0.6}\text{Sr}_{0.4}\text{TiO}_3$ (BST) and poly(methyl methacrylate) (PMMA) were analyzed at different solids content for drying behavior after DOD printing on PET (Figure 15).

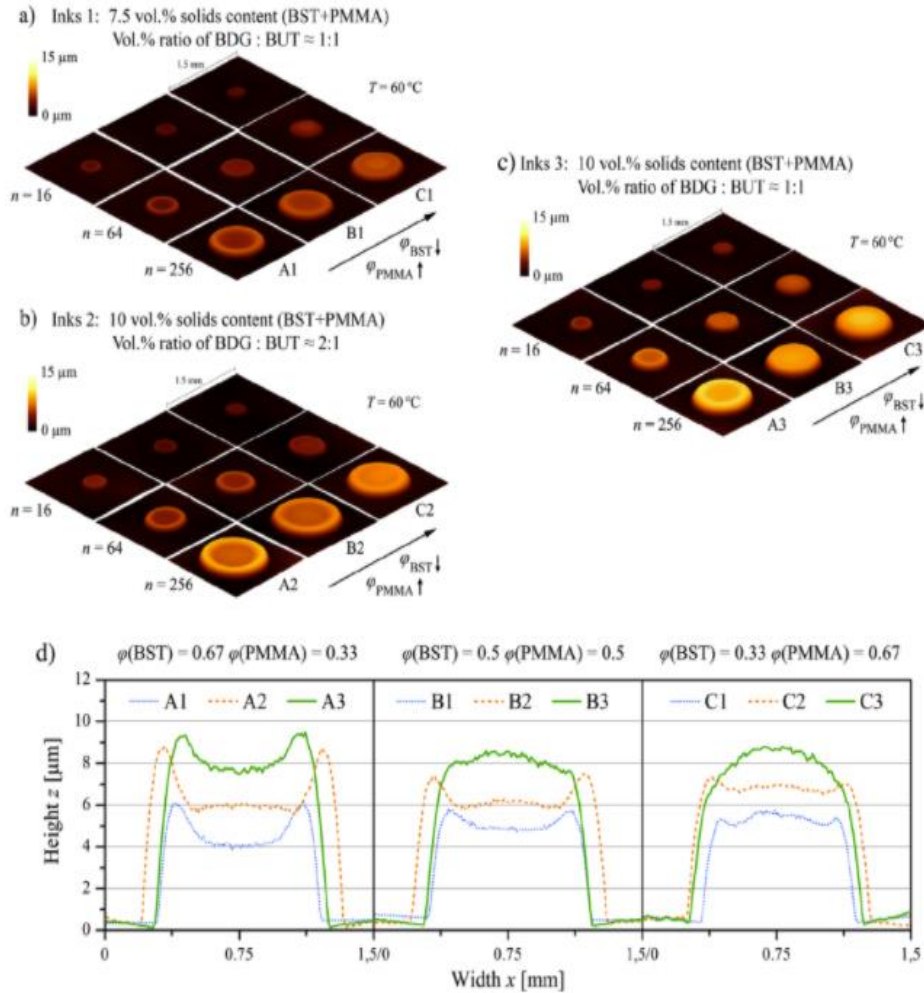


Figure 15: Topography of printing drop structures of different sizes dried at 60C on PET substrate (a, b, c) and cross sectional profiles of dried drop structures of the composite inks ($n=256$)

Topography imaging of dried the dried BST/PMMA drops show particle distribution is independent of butanone (BUT) solvent content. However, solutions with increased solid content retain structural morphology after evaporative drying but present differing drying behavior [42]. The drop structure profiles of different compositions are indicative of interaction between PMMA and BST dispersion within drops, rather than

hydrophilicity at drop edges resulting in homogeneous surface morphology of dried films from the in-situ ceramic/polymer solution (Figure 16) [42].

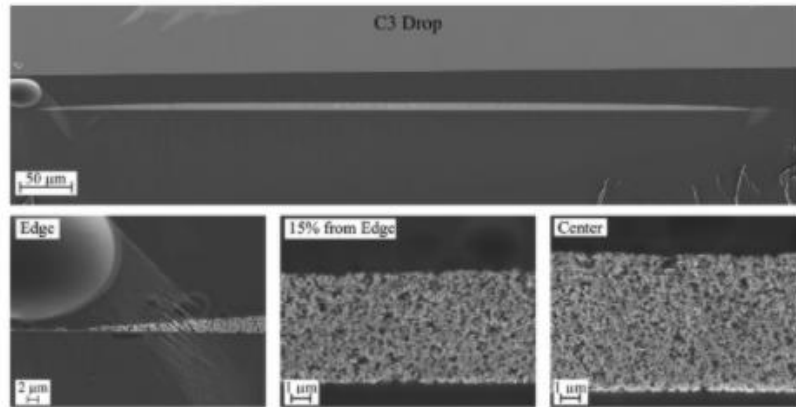


Figure 16: Cross sectional ion beam etched SEM images of printed drops after drying

Inkjet printing faces several pitfalls in scalability of thin film application, especially mixtures and/or constituents containing swellable clay materials. Additionally, large surface area printing such as in industrial application is difficult for inkjet due to time, space, and cost constraints.

3. PROPERTIES OF CLAY NANOCOMPOSITES

3.1 Thermodynamics

The thermodynamic stability of nanocomposites is dependent on the ability of polymer to maintain favorable interaction within the clay galleries. Modification of the clay surfaces is contingent on the phase states of both the polymer and clay nanoparticles and is critical to the degree of permanency and utility of the resultant composite. Control of experimental parameters such as the degree of layer separation of clay and interactions at surface structures ensures production of stable, functionalized nanocomposites with enhanced properties.

3.1.1 Structural Phases and Separation of Minerals

Nanocomposite morphologies of polymer-clay dispersions can be realized in the three discrete structural phases: agglomeration, intercalation, and exfoliation (Figure 17).

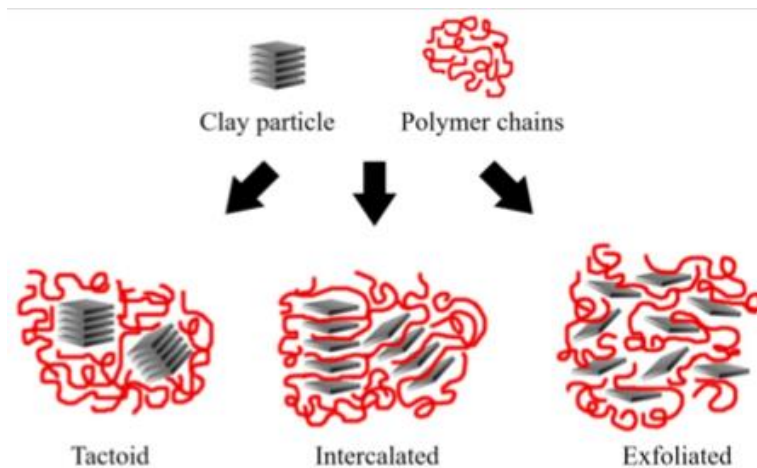


Figure 17: composite morphologies of polymer-clay constituent dispersions

Agglomerated or tactoid, composites present two distinct phases where clay sheets retain structure with no swelling in interlaminar space. In an agglomerated state,

clay dispersions remain aligned in parallel in the micron-ranged particulate size and reactive sites only at the platelet surface can undergo hydrogen bonding. Composites in an intercalated state (sometimes called flocculation) have polymer chains inserted between clay sheets that remain in highly ordered arrays. Although intercalated clays only have reactive sites on the platelet surfaces, increased interlaminar spacing via polymer inclusion similarly increases the number of available bonding allocations. Exfoliated nanocomposites are classified as clay sheets completely separated and thereby entirely dispersed within the polymer matrix.

Due to the high aspect ratio and exposure of each reactive site of individual platelets, fully exfoliated and well developed PCN structures effectively enhance mechanical properties such as tensile, compression and bending strengths when compared to neat polymer.

3.1.2 Self-assembly Behavior of PCNs with MMT

Self-assembly is an autonomous and spontaneous development of subcomponents into highly ordered patterned structures and well known in biological systems such as the striking example of DNA formation [20]. Emerging self-assembly processes relies on similar molecular architecture formation such as non-covalent interactions in templating surfactants or block copolymers [19]. Analogously, overcoming stacking forces between individual platelets of fully exfoliated MMT particles can be utilized as bottom-up templates which are highly ordered and easily dispersible in polymeric composite films. After complete delamination into singular silicate nanoplatelets, MMT form self-assembled, multilayered structured via solvent evaporation (Figure 18) [19].

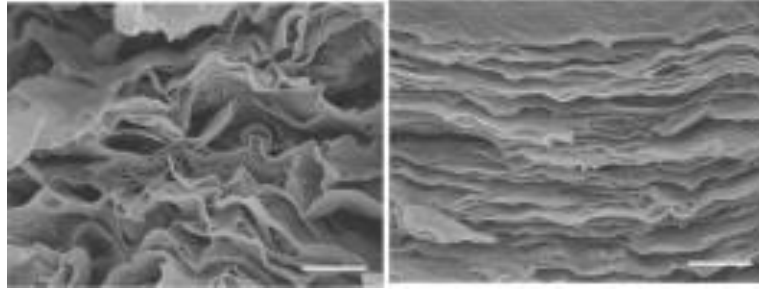


Figure 18 SEM cross section of MMT film before (a) and after (b) exfoliation and evaporation (scale bar: 2 μ m) [19]

Pure MMT's intrinsic layered structural distortion and reformation has been shown as a self-assembly process when hydrated and subsequently desiccated as seen in FTIR spectrum in Figure 19 [10].

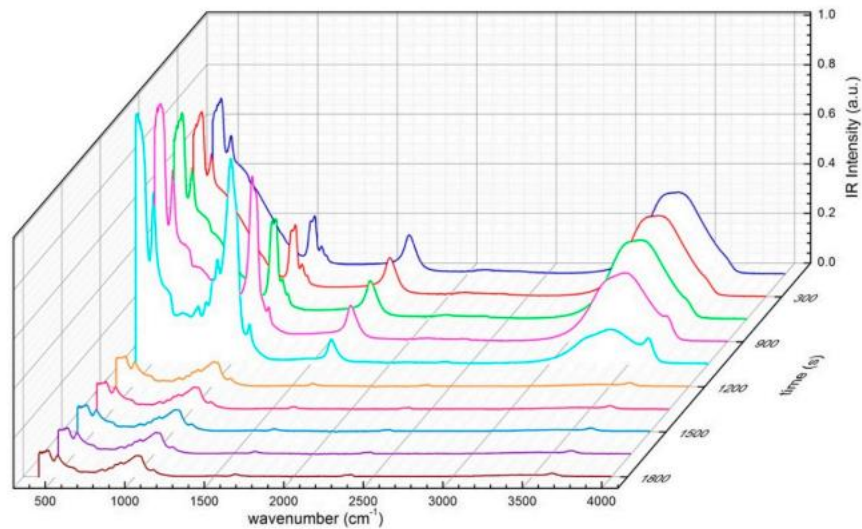


Figure 19: FTIR spectra of MMT-H₂O mixtures in the $400 < \Delta\omega < 4000 \text{ cm}^{-1}$ spectral range vs. time

The low frequency band at 3200 cm^{-1} is due to O-H vibrations of tetrahedrally bonded H₂O molecules, while high frequency 3400 cm^{-1} band can be attributed to O-H vibration of H₂O molecules with underdeveloped H bonding [10]. As the matrix becomes increasingly

dense with insertion of water molecules, hydrogen bonds become distorted as the packing arrangement reaches capacity limitations near 3400 cm^{-1} .

Supramolecular methodology during PCN formation depends on non-covalent interactions mediated by ion-dipole bonding at cationic sites of MMT surface. At exposed interfaces, organic cations effectively neutralize negative charge at interlamellar silicate, decreasing surface energy while improving wettability in the formation of polymer matrices in nanocomposites. The self-assembly mechanism of nanocomposites involving swellable clays is entropically driven in order to achieve thermodynamic equilibrium and reduce the system's free energy as such:

$$\Delta H = H(h) - H(h_0) = \Delta U - T\Delta S$$

Displacement of water molecules in the interlayers of MMT increases entropy as a consequence of polymer chains uncoiling and bonding at exchangeable cations sites (ΔH). The increasingly negative charged MMT gallery surface sites further restrict molecular chains of polymers represented by ΔU the configuration changes of various components. Initial (h) and final (h_0) separation of the clay interlayers whereby $\Delta H < 0$ therefore increases a favorable degree of intercalation [8]. This interlayer locking effect is known to increase tensile strength of the composition by resultant scaffolding. Versatile, water-soluble polymers such as polyvinyl alcohol (PVOH: $[\text{CH}_2\text{CH}(\text{OH})]_n$) have extended alkane chains that are able to further displace desorbed water molecules in bulk solutions which form tightly packed, ordered assemblies upon evaporation. This self-assembly procedure for the formation of intercalated nanocomposites presents in several orientations: most commonly, platelet face-to-face via ionic attraction (intermolecular forces) as well as edge-to-edge via non-polarity in organic solutions (hydrophobic effect).

3.1.3 Cohesion/Surface Energy

Damage resistance and deformation mechanisms of thin composite coatings present difficulties for analysis, where fracture non-linear geometries can present differently for the same coatings undergoing different mechanical stress [49]. These differences can be accounted for in surface and adhesion parameters by varying the degree of dispersion of fillers and mechanical reinforcement of PCNs. PCN formulations must present cohesive strength via intermolecular attraction such as hydrogen bonding and Van Der Waal forces and often presented as surface tension or, wettability. PCNs applied as surface coatings should also present adhesive strength, whereby sufficient attraction between coating and substrate creates interfacial tension, improving the mechanical properties of the system. According to Young's equation, the relationship between the contact angle (θ), the surface tension of the liquid (σ_l), and the interfacial tension between liquid and solid (σ_{sl}) and the surface free energy of the solid (σ_s):

$$\sigma_s = \sigma_{sl} + \sigma_l \cdot \cos\theta$$

Surface energy for solids can be predicted by Neumann's equation for the interfacial tension:

$$\sigma_{sl} = -2\sqrt{\sigma_l \cdot \sigma_s} \cdot e^{-\beta(\sigma_l \cdot \sigma_s)^2}$$

The thermodynamic work of adhesion at the clay-polymer interface can be accounted for with the Hamaker constant (A), an indication of the Van Der Waals interaction:

$$A = \pi^2 C \rho_1 \rho_2$$

Adhesion studies and Hamaker constant can be used to estimate the attractive forces between the number of densities of interacting clay platelets ($\rho_1 \rho_2$) and the mechanical force required to for delamination during processing [51].

Thermodynamic work of adhesion was shown to enhance mechanical properties of the Na-MMT organically modified with four different phosphonium surfactants yielding organoclays Ph1-Ph4. Clays with surface energy similar to that of the polymer exhibited low interfacial tension values and corresponding increase in modulus and work of adhesion (Figure 20).

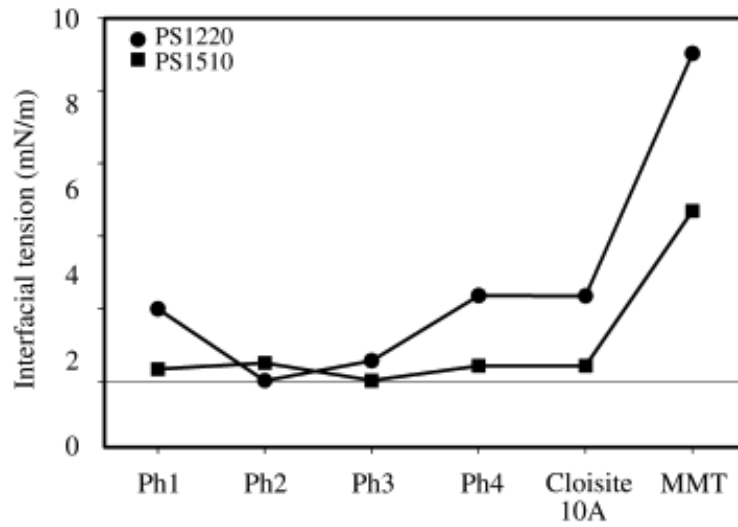
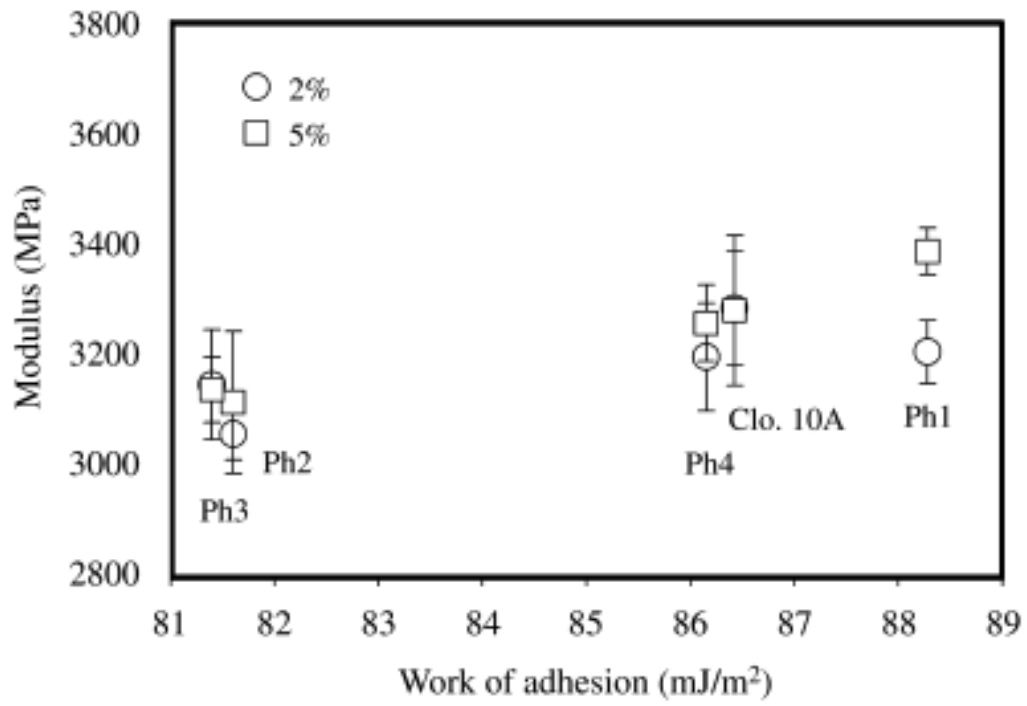
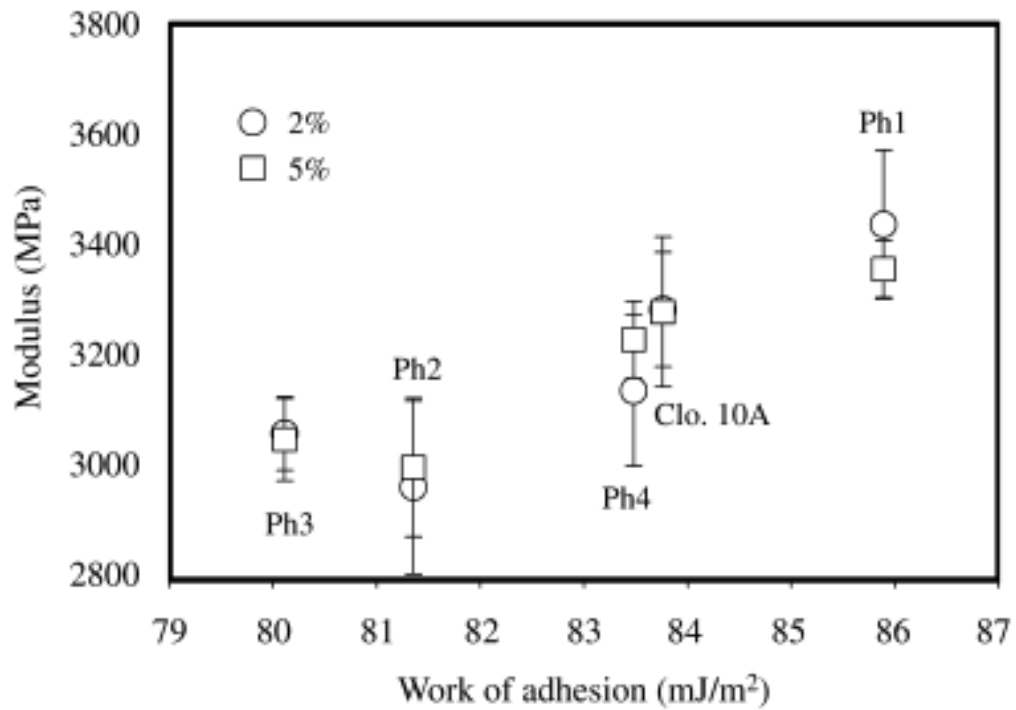


Figure 20: Interfacial tension of PS-clay systems at room temperature

Modulus increased at the clay-polymer interface as a function of adhesion (Figure 21). Additionally, modulus was demonstrated positively affected by quality of clay dispersion and degree of intercalation or exfoliation [50].



(a)



(b)

Figure 21: Influence of thermodynamic work of adhesion at room temperature on the modulus of nanocomposites (a) PS1510 and (b) PS1220 prepared with organoclays at two concentrations of clays

3.2 Mechanical Properties

In thin film coatings of PCNs, resistance to damage is controlled by the mechanical properties of the coating, interface, and substrate. Mechanical response of the system must be adequately accounted for and properly characterized for full functionalization of their intended applications. As the coating complexity increases (as with multilayered, multifunctional coating/substrate systems) so do the modes of deformation or failure, and thus, the response of finite elements must be considered.

3.2.1 Tensile Strength

PCNs synthesized with optimized polymer distributions yield enhanced mechanical characteristics such as increased tensile strength [9]. Mechanical performance is reflected in part by Young's modulus which is representative of a thin film coatings ability to withstand changes in length under lateral tension. The Young's modulus is a function of stress-strain slope equation:

$$E = \frac{\sigma}{\varepsilon}$$

Where,

$$(\sigma) = F/A , (\varepsilon) = \Delta L/L$$

Whereby the Young's Modulus (E) of a material is observed as the tensile stress (σ)/strain (ε) fraction in pressure units of Pascals (Pa). Tensile stress (σ) is calculated as the uniaxial force (F) applied per surface area (A). Tensile strain (ε), or total change in length (ΔL) over the initial length (L) is representative of the deformation of material. Young's Modulus (also called elastic or tensile modulus) is a characterization of the resilience of a material as it undergoes structural distortion. The thickness (T) of isotropic

samples enduring linear distortion (ε) has an inverse relationship as the cross-sectional area increases, the thickness proportionately decreases, as defined by Poisson's ratio:

$$P = \frac{\Delta T/T}{\Delta L/L}$$

However, platelet clays are anisotropic in nature and even more so when utilized in nanocomposites where polymer distribution can be in excess at individual particles. Evaluating mechanical properties of nanocomposites requires several critical considerations: volume fraction of dispersed phase, directional orientation of clay particles as compared to the strain vectors, and degree of interfacial association of polymer to clay.

The Halpin-Tsai model is a predictive elasticity calculation, accounting for both the geometry and orientation of filler in anisotropic dispersed-phase nanocomposites [14]. The estimation of reinforcement factor (ξ) and transverse stiffness (E_2) of the composite based on the Young's modulus (E_m) and volume fraction (V_f) of the polymer and modulus of clay (E_f) as such:

$$\frac{E_2}{E_m} = \frac{1 + \xi n V_f}{1 - n V_f}$$

Where,

$$n = \frac{E_f/E_m - 1}{E_f/E_m + \xi}$$

The aspect ratio of clay particles can be subsequently added to derived equations, implying the Halpin-Tsai equation can account for morphological changes of reinforced

composite matrices in the orthogonal direction of applied stress and resulting in an increased modulus [15].

Polyvinyl alcohol (PVA) has high tensile strength and flexibility, and in combination with MMT has been shown to successfully reinforce polymer nanocomposites in higher weight contents (30-70%). Figure 22 presents tensile strength of MMT/PVA nanocomposites as a function of clay content.

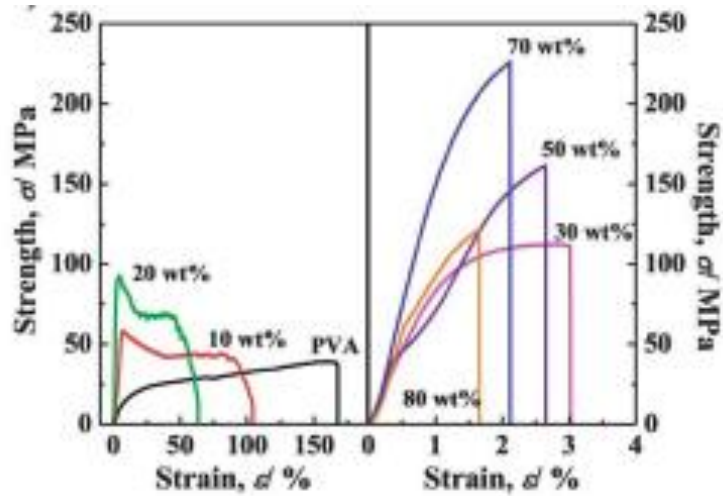


Figure 22: Tensile testing of MMT/PVA nanocomposites as a function of MMT content

In regions of relatively low volume fraction of MMT (0-16% region) illustrate a sharp increase in mechanical strength of polymer nanocomposites; 71 GPa at 4.7 vol% MMT resulting in a modulus increase of 12.3 times that of neat PVA (Figure 23) [16].

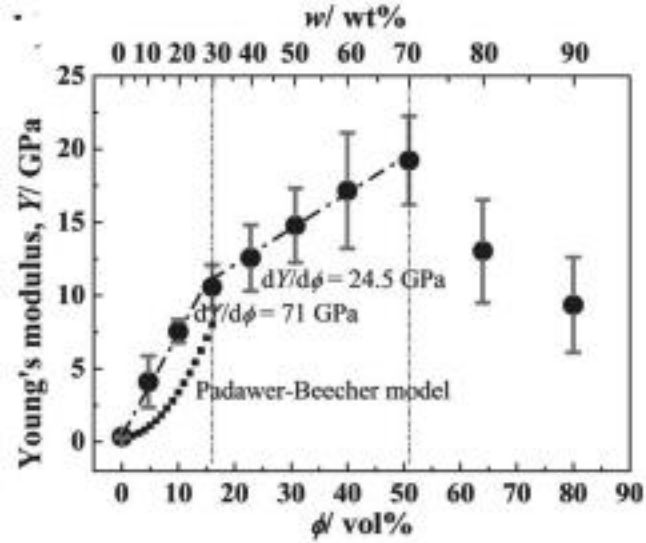


Figure 23: Stress-strain curve of MMT/PVA composites as a function of MMT weight and volume fraction

However, the steep increase in mechanical performance in lower loadings (0-30%) has been proposed to derive from a random amorphous structural assembly where the crystallinity of the polymer decreases as the constrained region increases. As the MMT weight fraction is increased (30-70%), nacre-like, organized structures prevail, as seen in SEM images of 10%, 30%, 50%, and 70% MMT/PVA (Figure 24). Well-defined layered structures are observed at MMT loading of 30% and higher.

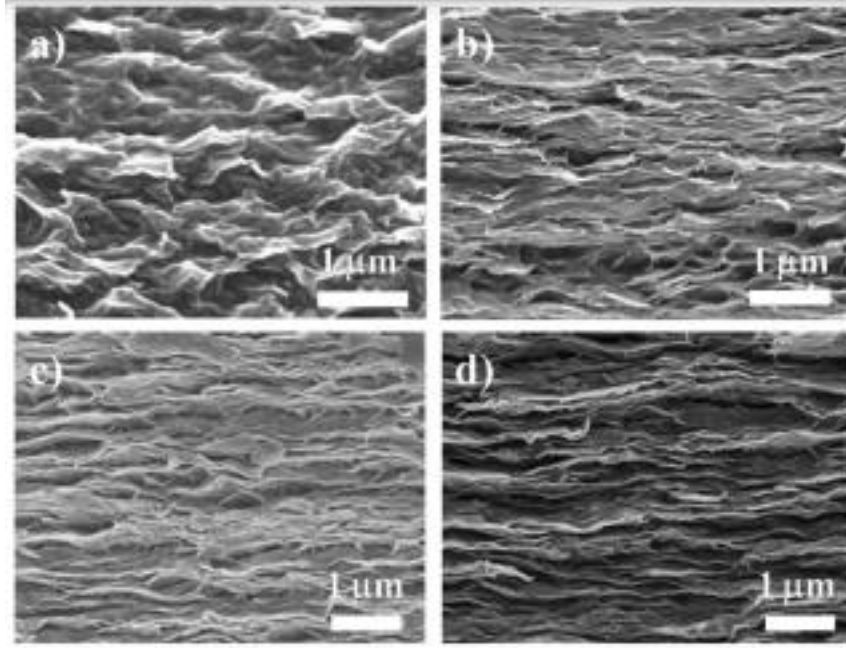


Figure 24: SEM images of MMT/PVA cross sections at 10% (a), 30% (b), 50% (c), and 70% (d)

Mesomechanical modeling of intercalated versus exfoliated nanoclay composites concludes mechanical strength and durability of fully exfoliated PCNs are higher than similarly intercalated species even at low (1-3%) weight fractions. As seen in Figure 25, intercalated (a) composites show lower toughness at three strain rates and three weight fractions as compared to exfoliated (b) composites within the same parameters.

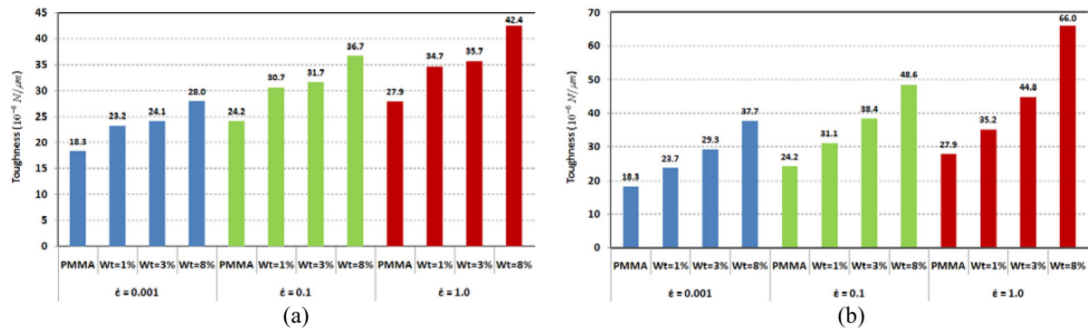


Figure 25: Strength comparisons of intercalated vs. exfoliated nanoclay composites [17]

Additionally, the deformation and failure modes of exfoliated PCN have been shown to withstand greater damages both in simulation and experimentally due to ability of exfoliated nanostructures' ability to distribute damage into localized bands (Figure 26). The 2-D representative volume element (RVE) model is used to prove overall characteristics of consistent surface elements at 1.0 /s strain rate for 1% (a, b) and 3% (c, d) clay loading at intercalated (a, c) and exfoliated (b, d).

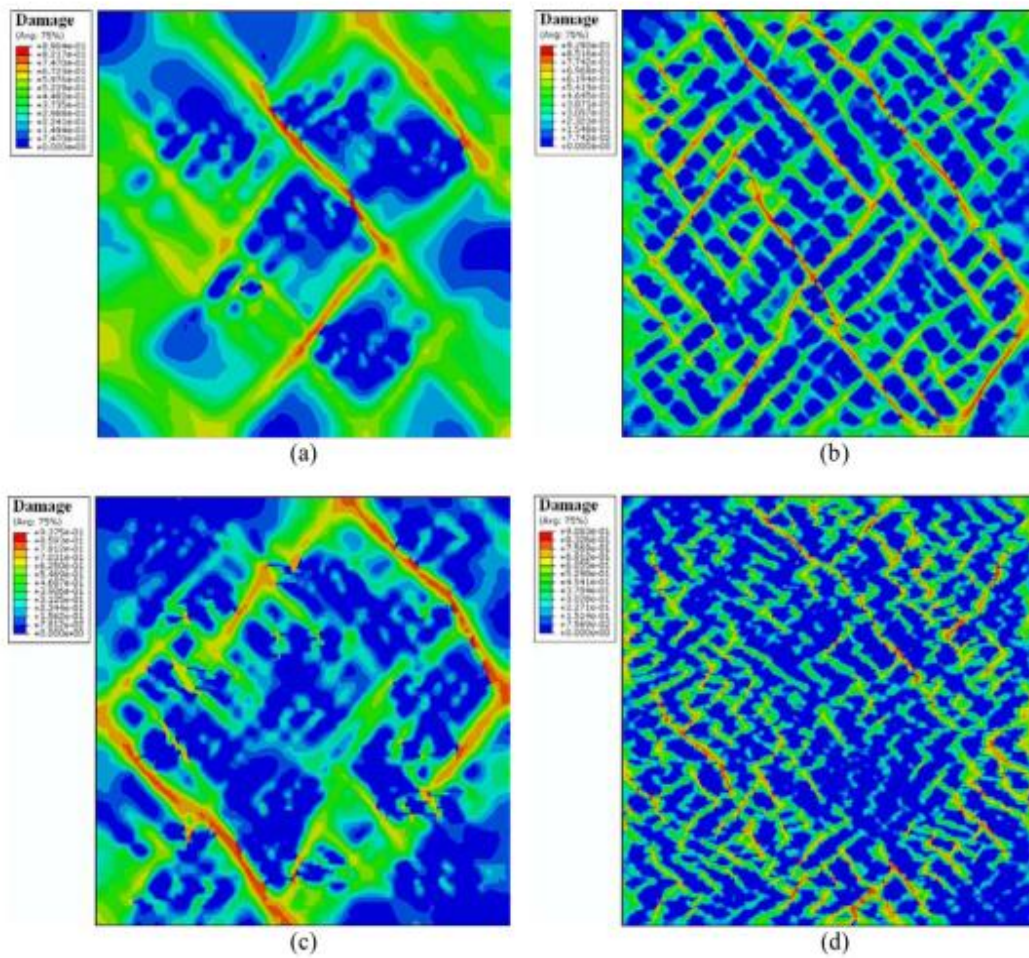


Figure 26: RVE damage distribution in nanoclay composites [17]

Therefore, polymer matrices with low weight fractions of well dispersed or exfoliated clay particles show enhanced stress-strain response in PCNs.

3.3 Thermal Properties

PCNs thin films synthesized with high aspect ratio clay particles report thermal stability, due to low conductivity of appreciable air entrapment within nanostructures. Isothermal TGA experiments of the resins and nanofillers have shown ammonium and phosphonium organo-modified clays show significant increase in stability as compared to neat MMT (Figure 27) [50].

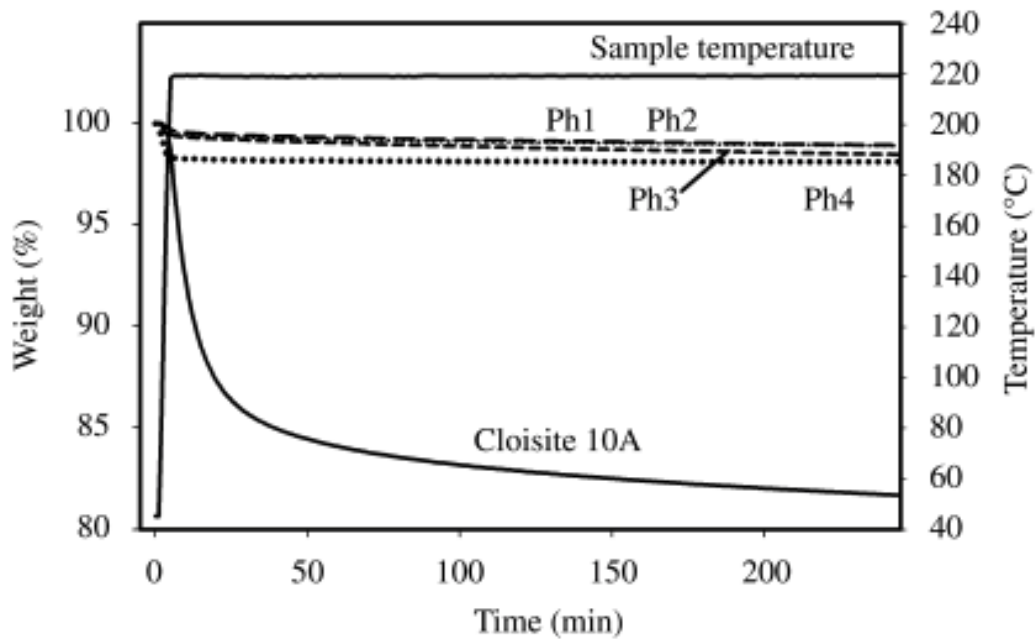


Figure 27: Thermal stability of organo-modified clays

Similar experiments of polystyrene-clay nanocomposites treated with ammonium and phosphonium salts observed thermal degradation which has been attributed to ammonium cation replacement on the clay surface. This follows the Hofmann elimination

mechanism (Figure 28) as tertiary amines and olefin are produced from the treatment of quaternary ammonium [52].

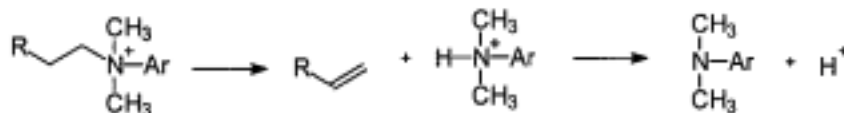


Figure 28: Schematic of Hofmann elimination as onium salt degradation produces an olefin, an amine, and a counterion on organo-modified clays

3.4 Barriers Materials

High-performing and low-cost anticorrosion surface treatments have become increasingly important across many industries in recent years. Thin film PCN LBL barriers have been demonstrated as conformal, high transparency fortification agents for protection against harsh atmospheric conditions such as contact with combustion, oxidation, high acidity, and radiation.

3.4.1 Chemical Resistivity

Another beneficial effect of increased aspect ratios of composite-incorporated clays is their utility as water or chemical adsorption barriers. Functionalized PCN coatings can be modified to minimize liquid and gas transmission to underlying substrate or surfaces.

MMT-filled, polyester-based nanocomposites present chemical resistance properties and can be measured in accordance with ASTM D543-87. By this methodology, weight fluctuations of composites are analyzed as a function of continuous contact with various solvents, as seen in Figure 29. Ideal constraints of functionalized MMT in PCNs is largely dependent on interactions within the clay galleries upon evaporation.

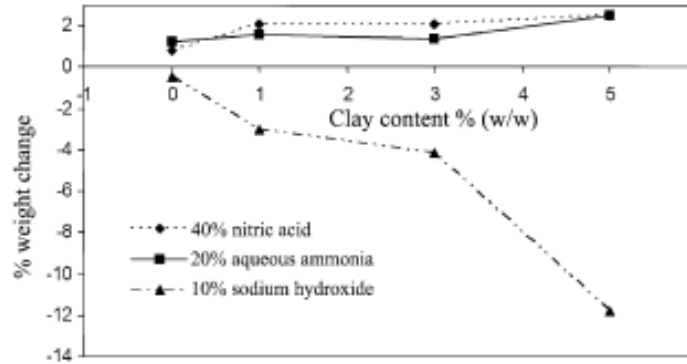


Figure 29: Δ weight of composites with varying MMT content in solutions [18]

Within the 0-5% wt of clay, weight gain after contact with solvents denotes expansion in clay due to interstice absorption of aqueous solvents. Weight loss indicates cation exchange within the MMT matrices with lighter ions. The sharp decrease in weight observed with NaOH is weakening the interfacial adhesion of the PCN as inorganic cations such as Na^+ and Ca^{2+} are exchanged with organic cations, thus rendering the clay progressively more hydrophobic.

Charge transfer resistance (R_{ct}) is an important barrier property correlated with corrosion resistance as it relates to electrochemical reactions on substrate surfaces [53]. Anti-corrosion studies of PCN films composed of branched polyethyleneimine (PEI) and glutaraldehyde (GA) crosslinked MMT clay platelets deposited by LBL process revealed increased barrier properties of films even when immersed in corrosive environments.

Electrochemical measurements of PCN-coated steel coupons exposed to 0.6M NaCl solutions aqueous saline immersion by Bode magnitude plots (Figure 30).

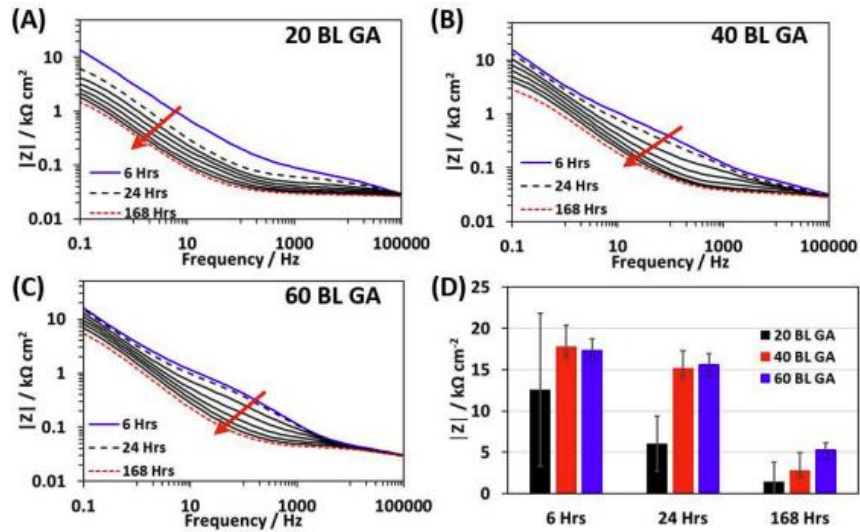


Figure 30: Bode impedance plots from GA-crosslinked PCN-coated steel coupons in bilayers applications of (a) 20, (b) 40, and (c) 60 over 168 hours. Bar graph (d) shows low frequency impedance (0.1 Hz) value for each thickness over time

Results show the corrosion inhibition is dependent on the number of bilayers applied, as they increase R_{ct} as diffusion of electrolyte is impacted by film barrier [54].

Electrochemical response of PCN film immersed in solutions comparable to sea water could prove low-cost alternatives as corrosion and resistivity inhibitors in aqueous environments.

3.5.2 Gas barriers

Thin layers of PCN material have been shown to produce high barrier performance to oxygen and other gases and vapors. In the flexible electronics industry, an estimated oxygen transmission rate (OTR) below $10^{-5}\text{ cm}^3/(\text{m}^2/\text{day}/\text{atm})$ are required for resilient organic light emitting diodes (FOLEDs) [44]. In order to improve the gas diffusion properties of PCNs, the pathway within the polymer matrices must be either

increased in length and/or in complexity. In a more complex pathway, a permeating molecule such as oxygen, is forced to travel an extensive diffusion path when highly aligned clay platelets with high-aspect ratio are incorporated into polymer matrices [45]. This complexity is caused by clay nanoparticles creating a maze through which the permeant must travel as is represented as the tortuous path model (Figure 31) [46].

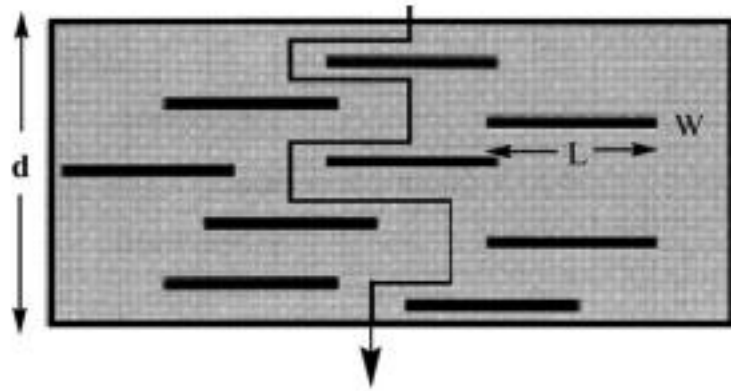


Figure 31: Tortuous Path model of clay platelets in polymer nanocomposites

This theory only takes into account the aspect ratio of the clay plates and the volume fraction of the filler in the 2D composite and can be calculated in with Nielsen's equation for permeability:

$$\frac{P_f}{P_u} = \frac{V_p}{1 + \left(\frac{L}{2W}\right) V_f}$$

The permeability coefficient of the composite (P_f) and the permeability coefficient of the pristine polymer (P_u) can be estimated from the volume fraction of the polymer (V_p) and the filler (V_f), the average length (L) and thickness of the filler (W). Nielsen's model predicts the permeability behavior of a systems with low clay loadings (>1%) [46].

The tortuous pathway has been shown to significantly extend permeating molecule's diffusion times as well as lower the gas transmission rate as seen in Figure 32 [45]. The OTR of thin film assemblies of polyvinyl amine (PVAm) polyvinyl amine (PVAm), branched polyethyleneimine (PEI), poly(acrylic acid) (PAA) and sodium montmorillonite (MMT) clay was decreased by two orders of magnitude while only increasing thickness of neat PET substrate by ~0.04%. Permeability is shown decreasing as a function of quadlayers or, exponential LBL assemblies, deposited and a 175nm thick (PVAm₁₀/ PAA₄/PVAm₁₀/MMT)₆ coating has a permeability comparable to metalized plastic film while remaining transparent.

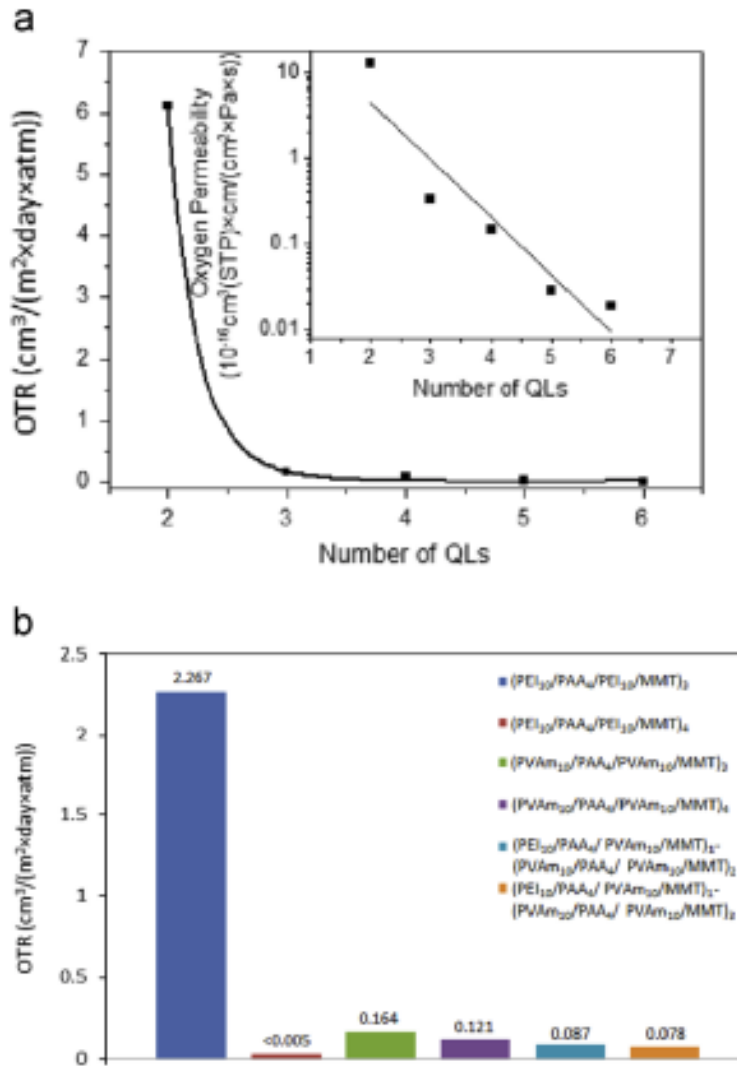


Figure 32: (a) OTR and permeability as a function of PVAm-based quadlayers deposited on PET and (b) as a function of quadlayer recipe and number of depositions

In accordance with the orientation of clay particles in nanocomposites of the thin films, Cussler's model can be applied to qualitatively describe the mechanisms of alignment within the polymer matrix:

$$P_0 / P = 1 + \mu\alpha^2 (\varphi^2 / 1 - \varphi)$$

Where the polymer permeability (P_0) over the composite permeability (P) is a function of the aspect ratio of the clay particles (α), as well as the geometric factor (μ) and volume

fraction (φ) of the composite [47]. The Cussler model is consistent when assuming the clay loading as proportional limits of dilution [48], whereby:

$$\varphi \ll 1 \text{ and } \alpha\varphi > 1$$

3.5.3 Flame retardants, heat shielding, and insulation

Demand for polymeric coatings that meet increasingly stringent fire regulations are becoming more desirable as flame propagation control and smoke produced from burning organics on surface coatings of conventional fireproof materials are falling short of new standards [21].

Efficacy of heat shielding properties of thin films (20 to 100 μm thick) consisting of pristine MMT as compared to particles exfoliated by polyamine salts were evaluated against continuous flame over time. Interestingly, lower thickness (20 μm) NSP (nanosilicate silicate platelets) outperformed thicker (100 μm) films (Figure 33) [19].

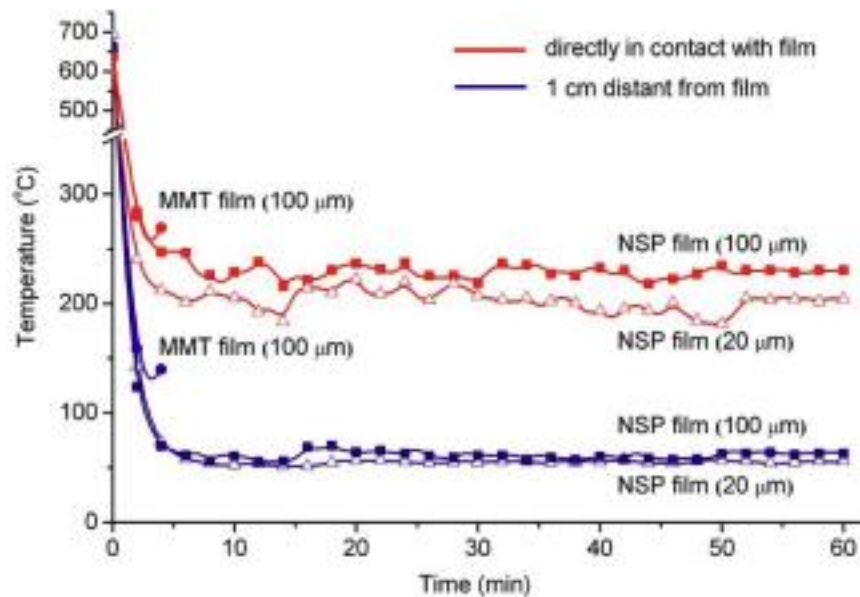


Figure 33: Heat shielding abilities of clay films exposed to flame at different distances and temperatures over time

It was hypothesized that increased heat shielding efficacy of direct flame contact with 20 μm films is attributed to their low thermal conductivity ($0.17 \text{ Wm}^{-1}\text{K}^{-1}$) and the volume fraction of the air voids in the alternating layers of the nanostructure as illustrated in Figure 34 [19].

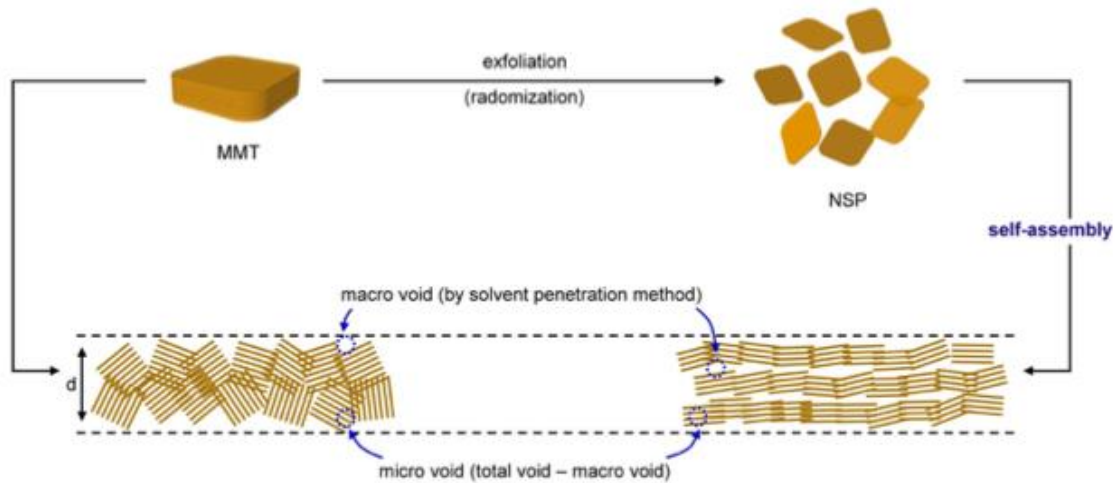


Figure 34: Conceptualization of air voids in fundamental units of multilayered structures of NSP and MMT films

The contribution of alternating macro voids produced from compounding layers of platelet-platelet stacks contributes to the total volume-air void composition which affects the film's ability to block gas, heat, and flame.

Similarly, nanocomposites with low clay loading (0.1-3%) were shown to decrease the peak heat release rate (PHHR) as compared to virgin polymer (Figure 35).

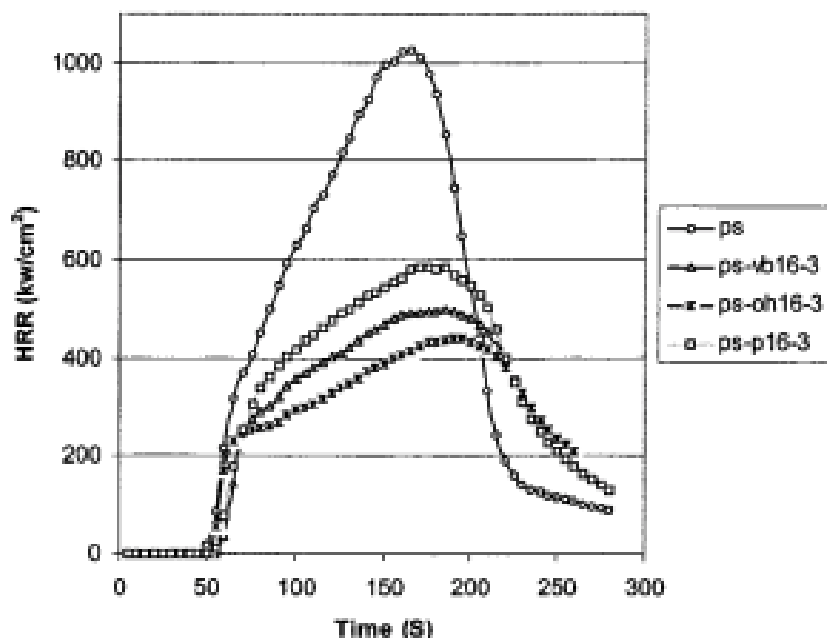


Figure 35: Peak heat release rates for polystyrene polymer and three nanocomposites

The suggested mechanism of clay nanocomposites decrease of PPHR involves char formation of PCN which serves as a mass and energy transport barrier [52].

3.5 Optical Properties

PCN coatings have also been demonstrated as optical filters to improve light transmission of surfaces in industrial and scientific instruments [55]. Anti-reflection (AR) PCN coatings produce low refractive indices and high optical transmission as a function of number of layers and clay-polymer fraction. Reflection within multiple internal layers causes interference within the thin film, whereby multilayered PCNs arise as AR functionalized coatings.

Hydrothermally treated synthetic smectite clays shows production of waved polymer crystal growth, yielding highly flexible films with tunable transparencies [56].

The structural characteristics of clay particles in PCN films owing to flexibility and transparency are modeled in Figure 36.

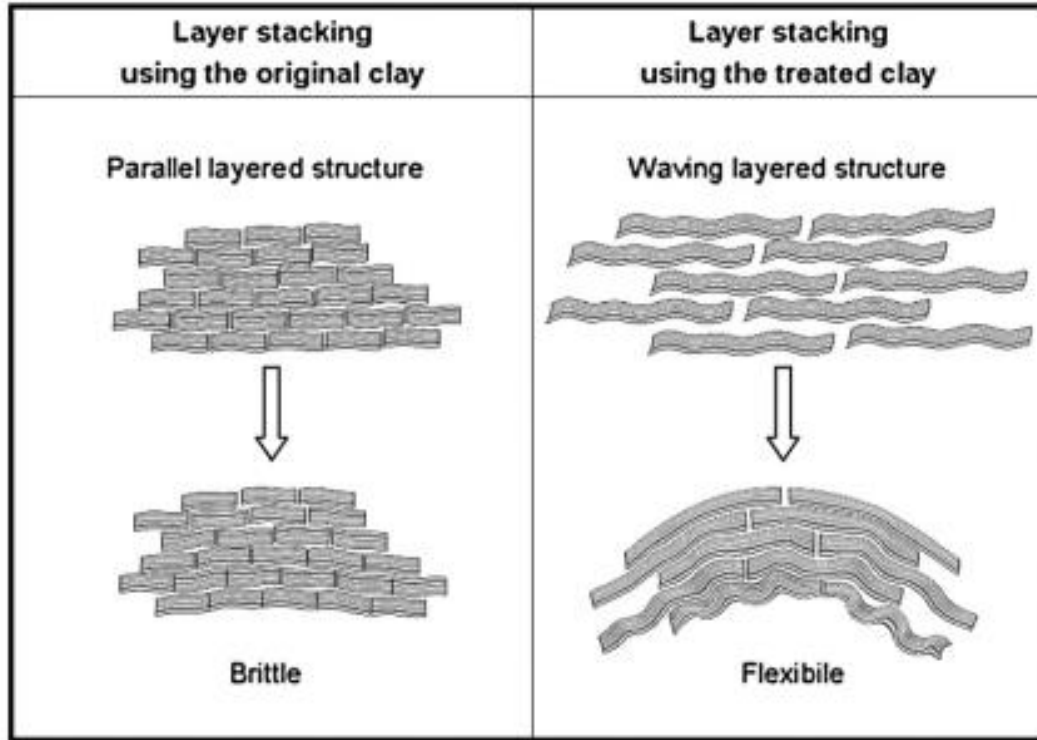


Figure 36: Structural scheme of original versus hydrothermally treated clay particles and their behaviors

Visible light transmission has been shown unaffected in corrosion applications of layered PCN thin films. When applied as an anticorrosion barrier on copper coupons, PCN films show optical reflectance follow corrosion performance trends, maintaining visual appearance and degree of sulfidation with corrosive exposure (Figure 37).

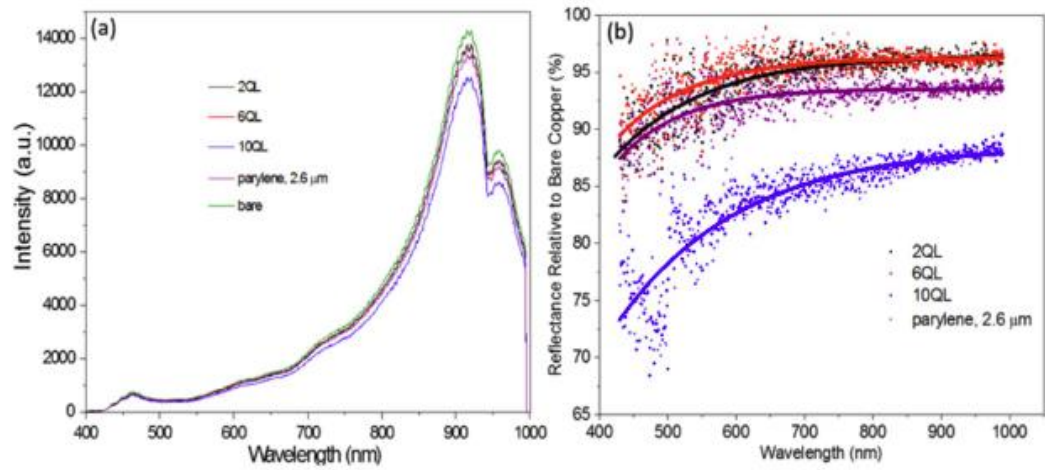


Figure 37: Reflectance intensity of PCN coating on copper plates (a) and measured reflectance relative to bare copper (b) via UV-VIS spectroscopy

The integrity and efficacy of PCN depositions were shown as protecting copper plates from electrochemical kinetics of copper sulfidation by lowering permeation rate while retaining optical properties of copper substrate [43]

4. POLY(VINYL ALCOHOL)/MONTMORILLONITE NANOCOMPOSITE THIN FILMS

4.1 Introduction

Poly(vinyl alcohol) (PVOH or PVA) is a synthetic, hydrophilic polymer known for its low cost, nontoxicity, biocompatibility and partial biodegradability, high hydrophilicity and excellent chemical resistance [60]. Furthermore, its exceptional physicochemical stability, film-forming features and optomechanical properties have enabled its applicability as an antifouling additive for commercial filtration membranes [61]. PVOH is produced from hydrolysis of polyvinyl acetate by replacement of ester vinyl acetate by hydroxyl groups and cannot be produced from polymerization vinyl alcohol which will rearrange to the more stable acetaldehyde (Figure 38) [64].

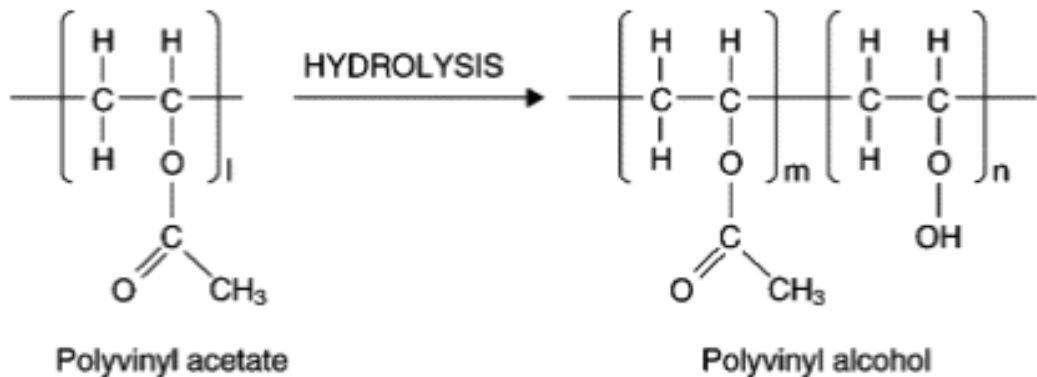


Figure 38: Hydrolysis reaction mechanism yielding polyvinyl alcohol

PVOH is also the most common pigment binding agent used in inkjet coatings because of its molecular structure, which allows hydrogen or ionic interactions with

chemical groups of PVOH which become trapped within the network structure after water evaporation (Figure 39) [62].

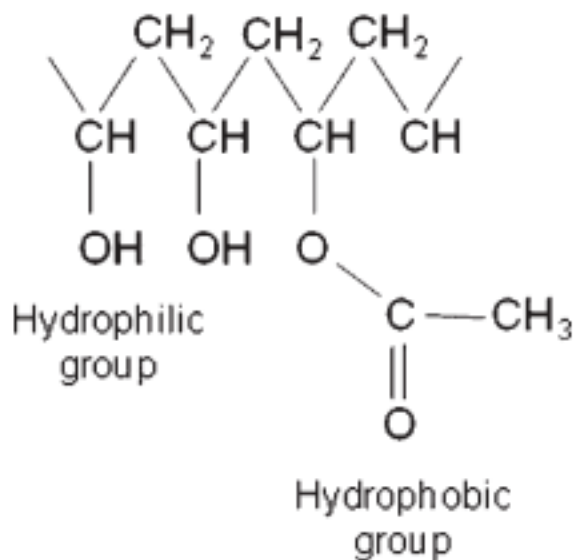


Figure 39: Chemical structure of polyvinyl alcohol

PVOH contains vinyl alcohol and vinyl acetate groups and has crystalline and amorphous parts of the structure depending on the degree of hydrolysis within the polymer matrix [63].

PVOH thin films produced in different time and temperature conditions found crosslinking behaviors were optimized at elevated temperature and relatively shorter mixing times. The optical absorption behaviors of the varying preparation techniques yielded optical activity where UV-Vis absorption spectra indicate the increase in processing temperature increases the emission intensity absorbance (Figure 40) where S5 (180°C, 65 min) is reduced at 280 and 335nm and optimal crosslinking occurs at S4 (180°C, 30 min) [65].

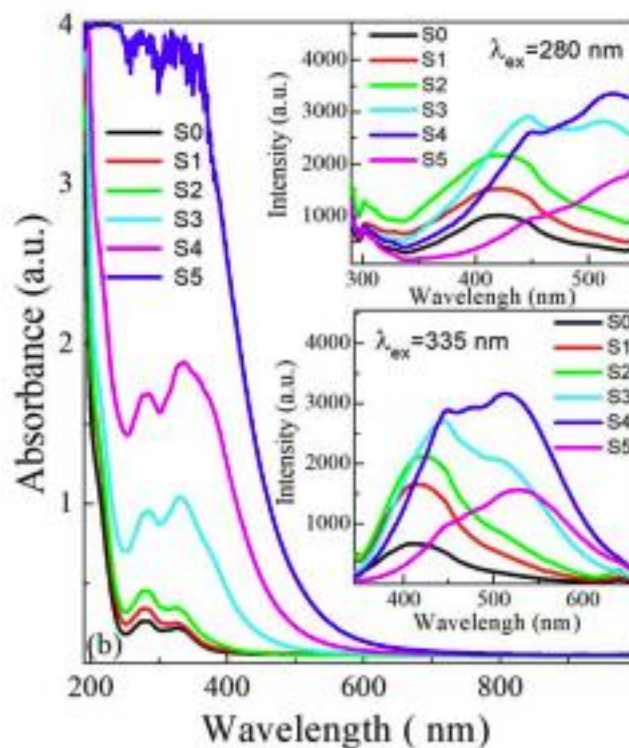


Figure 40: UV-VIS absorption spectra of S0 (neat PVA film), S1 (120°C, 80 min), S2 (140°C, 75 min), S3 (160°C, 70 min), S4 (180°C, 30 min), S5 (180°C, 65 min)

4.2 Experimental

4.2.1 Materials

PVOH (polyvinyl alcohol) 3-80: ELVANOL™ was acquired from Kuraray. PVA (polyvinyl acetate) 189480 and PVP (polyvinylpyrrolidone) K 90 acquired from Sigma-Aldrich. MMT (Montmorillonite; Cloisite Na⁺) and LAP (Laponite) was obtained via donation from BYK. Polyethylene terephthalate (PET) substrate, CG5000 was purchased from 3M.

4.2.2. PCN preparation

Isolated clay and polymer samples were prepared in DI water in varying ratios as well as in combinatory mixtures as seen in Table 3.

Table 3: PCN preparation by weight in DI water

Type	Component(s)	%
Polymer	PVP	0.3
	PVOH 3-80	0.3
Clay	MMT	0.45
	LAP	0.45
Pre-mixed	PVP / MMT	0.3 / 0.45
	PVOH 3-80 / MMT	0.3 / 0.45

Isolated clay solutions were mechanically mixed for 15 min at room temperature. Isolated polymer solutions of PVA and PVP were dispersed via magnetic stirring for 30 min at 125C. Combinatory “pre-mixed” polymer/clay mixtures were magnetically stirred for 30 min at 125C with isolated polymers first, then removed from residual heat and clays were integrated at room temperature and magnetic stirring for an additional 15 min.

PET substrate was prepared by cleaning and drying of the untreated surface with isopropyl alcohol before first PCN application.

4.2.3 Thin film applications

PCN were then deposited in LBL fashion to untreated PET substrates in either 12 or 24 layers using spray coating as seen in Table 4.

Table 4: PCN species and thin film applications parameters.

Type	Component(s)	%	# Layers (total)
Pre-mixed	PVP / MMT	0.3 / 0.45	12
	PVOH 3-80 / MMT	0.3 / 0.45	12
LBL poly + clay	PVP / MMT	0.3 / 0.45	24
	PVOH / MMT	0.3 / 0.45	24
LBL clay	LAP	0.45	12
	MMT	0.45	12
LBL poly	PVOH	0.3	12
	PVP	0.3	12

Due to the low viscosity and low loadings of the solutions, doctor blading and dip coating caused deformations during evaporation as a result of phase separation as liquids pooled on substrate surface, similar instances observed in LBL applications without dry time. All other LBL applications had dry times based unobservable movement on the surfaces.

Print solutions of polymers and clays were placed in Fujifilm Dimatix DMP-2831 cartridges (Figure 41).



Figure 41: Fujifilm Dimatix DM-2831 inkjet printer and cartridges

Cartridges contain 16 nozzles spaced 254 μm apart. Each nozzle of print head can generate a minimum volume of 1 picoliter (pL) in a single drop and can deposit features as small as 20 μm at 100 dpi resolution. Figure 42 shows forced streams of liquid from cartridge nozzles as compared to the size of a quarter.



Figure 42: Dimatix print cartridge nozzle sizes as compared to a quarter

In order to exit inkjet nozzles, solutions must be injected through 0.2 μm filter to fill the cartridge. Clay solutions were entirely separated from DI water through the filters and did not produce uniformly printed films as evidence by the color discrepancies after filtration and prints on substrate (Figure 43 and 44).

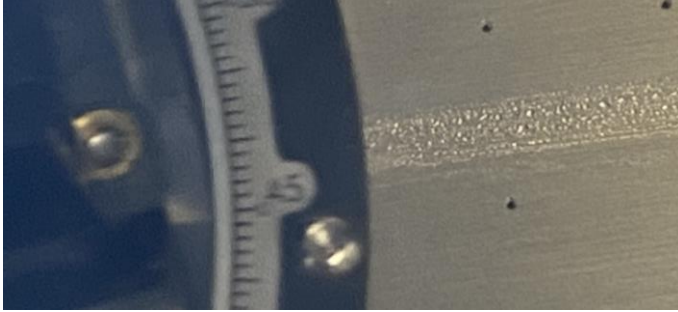


Figure 43: PCN film during printing, showing discrete droplets at non-uniform sizes

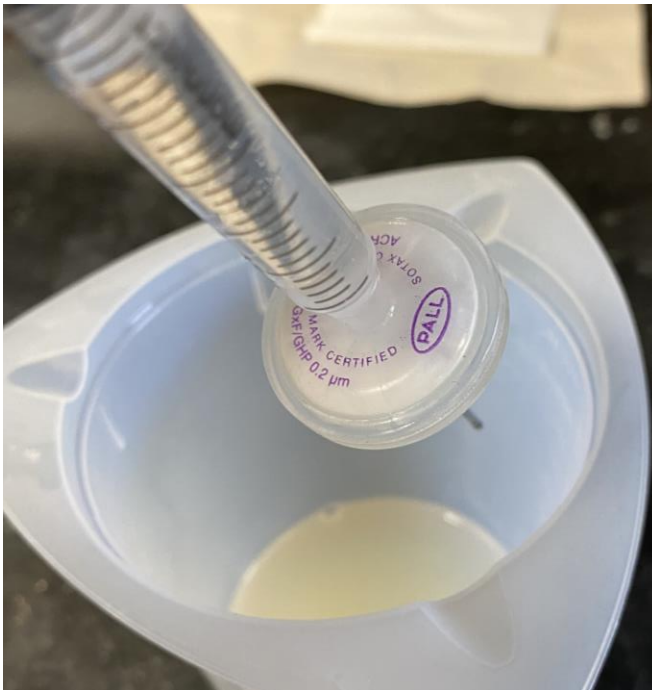


Figure 44: Clay before (in solution) and after (in syringe) filtration to demonstrate color change

4.2.4 Characterization

Mechanical tensile testing was performed using Materials Test System (MTS) Exceed E43 (Figure 45).



Figure 45: Mechanical tensile testing equipment used for thin films deposited on PET substrate

Commercially pre-treated side of PET was removed (reverse of PCN coating) either mechanically or chemically to diminish interference of unknown composite interference during characterization. Tensile samples were cut to 25.4 mm W. Starting sample lengths determined by space between instrument clamps and recorded. Total sample thicknesses were measured and recorded as an average of several locations (substrate + coating).

Photomicrography of completed PCN thin films was used to evaluate surface layer topography, general homogeneity of applications and deformation occurrences.

4.3 Data and Analysis

4.3.1 Mechanical testing

All PCN films show increased mechanical strength as compared to neat PET samples. The stress-strain curve of neat PET (Figure 46) indicates tensile data calculations (Table 5).

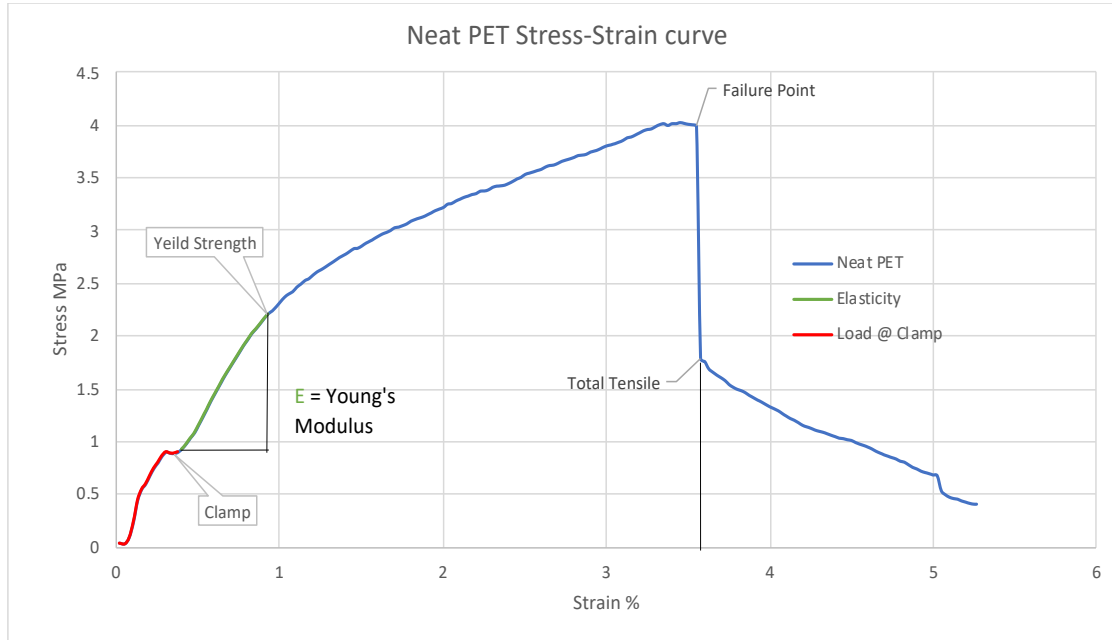


Figure 36: Neat PET Stress-Strain curve

Mechanical tensile testing performed on MTS did not include a pre-load force therefore, tension at clamp sites of the samples are signified in red and are not included in Young's modulus calculations. Young's modulus (E) values were calculated from the slope of the curve in green. Yield strength is the maximum force (MPa) the material can withstand before experiencing permanent damage and denoted by non-linearity in the curve as the material begins to deform. Total tensile strength of the material was found by integrating under the curve from Young's modulus to point of failure.

Increased yield strength and Young's modulus is seen for PVP 0.3%/LAP 0.45% as compared to PVOH/MMT at the same percentages and applied LBL for 24 total

applications. PVP/LAP LBL composition is shown as having the highest ultimate tensile strength of all films tested. This is expected of stiff polymer loading of nanoparticles as compared to the more ductile PVOH (Figure 47) and would indicate higher bonding strength between PCN layers and to substrate.

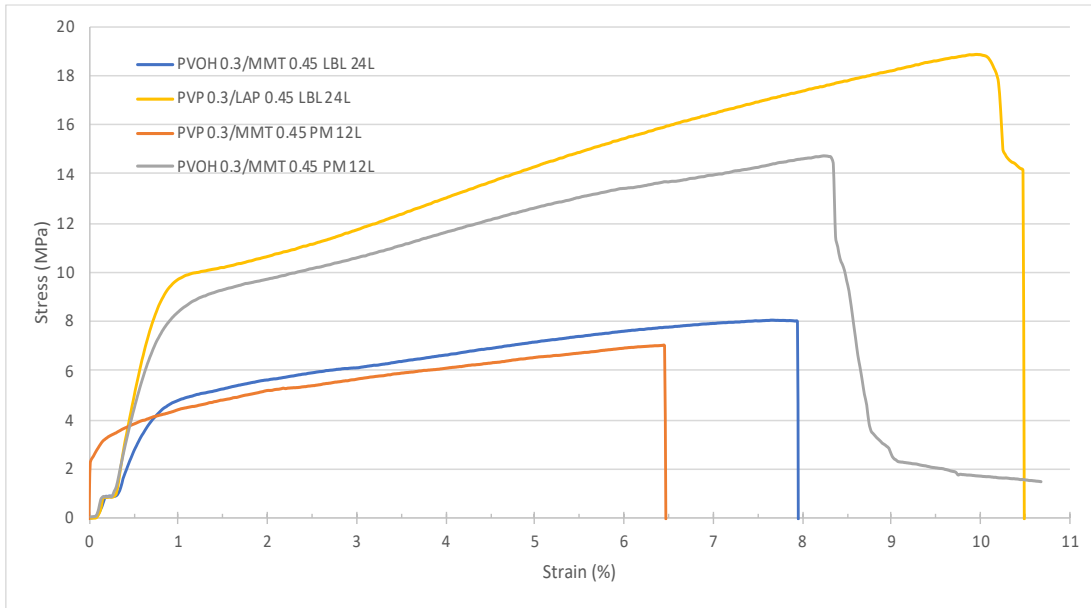


Figure 47: Stress-Strain curves of PCN applications of PCN in various combinations

Strain hardening is observed for all PCN applications as evidenced by the continued rise in stress-strain curves after yield point. This is caused by alignment of polymer chain molecules and lamellar crystals causing the material to strengthen during deformation. The elongation at yield for premixed PVOH/MMT and PVP/MMT 0.3%/0.45% respectively show stress/strain curves is to be expected as the system has become less brittle than clay only curves as polymer produces more ductile coatings, increasing the deformation capacity before fracture (Figure 47). Comparing relevant high-performing coatings to neat substrate shows enhanced mechanical properties among all PCN application types and species. Premixed PVOH 0.3/MMT 0.45 out-performed its

bi-layered counterpart even at half the number of applications. However, this is not applicable to premixed PVP/MMT PCN films of the same ratios and bi-layered coatings. PVP 0.3/LAP 0.45 in 24 layers is shown has having the largest impact on the tensile testing of the selected samples.

PCN films containing only MMT or LAP clay at 0.45% are shown with comparatively low maximum strain at break which is expected due to their inherent brittleness without polymer matrix interaction (Figure 48). Applications of only PVOH polymer at 0.3% are seen as improving mechanical properties of the system as compared to neat polymer, but not more so than independent clay applications (Figure 48).

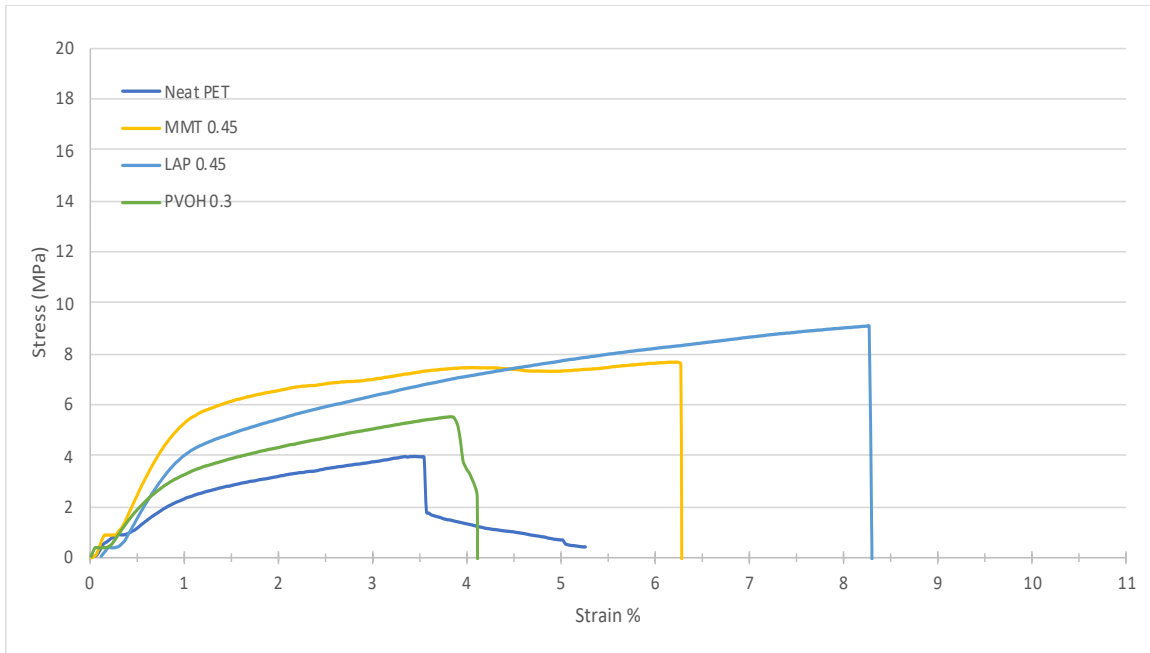


Figure 48: Stress-strain curves of solitary clay or polymer coatings as compared to neat PET

Table 5: PCN tensile values as compared to neat PET

Composition	%	Layers #	Deposition	Coating Thickness (mm)	Young's Modulus (MPa)	Increase from Neat PET (%)	Yeild Point (MPa)	Total Tensile	Failure Point (Strain @ Fracture) (%)
Neat PET					2.69		2.21	11.60	3.98
PVOH/MMT	0.3/0.45	24	LBL	0.05	7.08	163%	4.12	50.05	7.96
PVP/LAP	0.3/0.45	24	LBL	0.05	15.47	475%	8.43	144.46	10.00
PVOH/MMT	0.3/0.45	12	Premix	0.03	13.51	402%	6.97	100.17	8.48
PVP/MMT	0.3/0.45	12	Premix	0.04	6.71	149%	3.15	36.18	6.47
MMT	0.45	12	LBL	0.01	6.94	158%	4.68	39.55	6.29
LAP	0.45	12	LBL	0.02	5.54	106%	3.85	54.49	8.31
PVOH	0.3	12	LBL	0.04	4.60	71%	2.39	15.99	3.88
PVP	0.3	24	LBL	0.08	7.64	184%	3.72	97.37	12.19

4.3.2 Microscopy

PCNs from this study presented good over-all surface coverage of substrate area tested for mechanical properties. Imaging of bi-layered (Figure 49) and premixed (Figure 50) PVOH 0.3/MMT 0.45 at 12 and 24 layers respectively, reveals rough surface topography in both cases. Premixed appears to air bubble formation and may give rise to its ductility in mechanical testing.

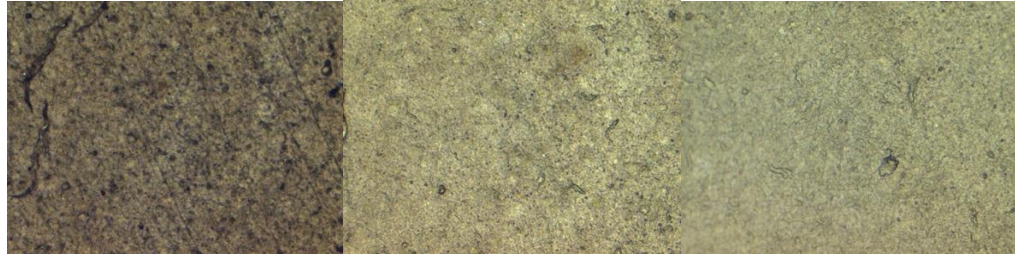


Figure 49: microscope imaging of PVOH 0.3 / MMT 0.45 at 24 layers at 5x, 10x and 20x resolution

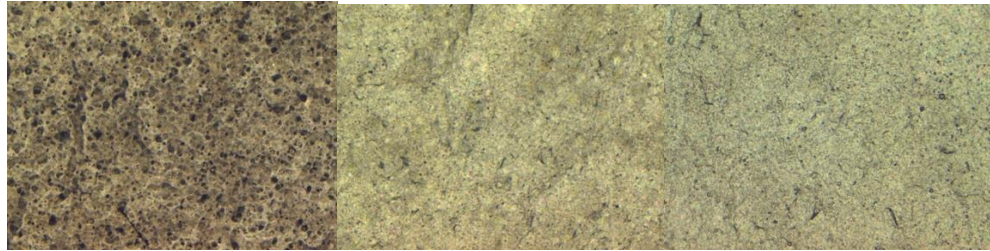


Figure 50: microscope imaging of Premix PVOH 0.3 / MMT 0.45 at 12 layers at 5x, 10x, 20x resolution

Imaging of PVP 0.3/LAP 0.45 at 24 layers (Figure 51) appears to have surface zones permitting of elasticity and fracture resistance.

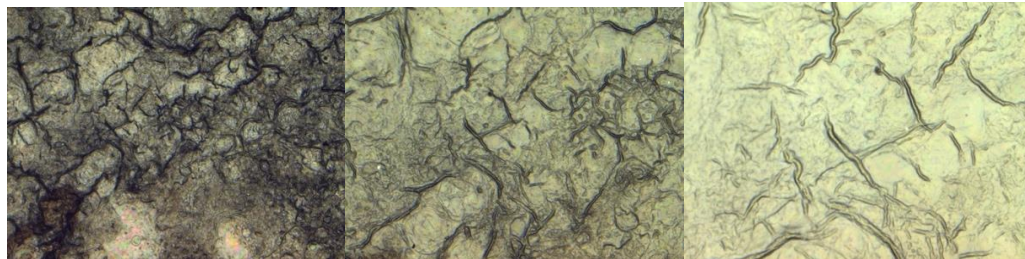


Figure 51: microscope imaging of PVP 0.3/LAP 0.45 at 24 layers 5x, 10x, 20x resolution

4.4 Conclusions

The use of MMT and LAP as reinforcement filler for PVP and PVOH polymers in PCN thin film spray coating applications improved mechanical performance as compared to neat substrate even at low loadings. Both premixtures and bi-layered depositions of PCNs were shown to substantially improve durability of the substrate while retaining flexibility of the system.

With minimal processing of both the neat polymers and clays, the PCN thin films resulted in highly effective performance materials easily scalable. Applicability to industrial and commercial needs is easily manageable for these PCNs, particularly for high-performance outcomes of premixed solutions applied via spray coating. Materials used to prepare such nanocomposites are readily available and yield enhanced performance, highly transparent thin films. The utility and functionalization of PCN can be of great value by incorporation or replacement of thin film packaging on the market today.

REFERENCES

- [1] Cristea, C.; Cristea, M.; Antucevičienė, J. KPIs for Operational Performance Assessment in Flexible Packaging Industry. *Sustainability (2071-1050)* **2021**, *13* (6), 3498.
- [2] Reddy, K. R.; Venkata Reddy, Ch.; Babu, B.; Ravindranadh, K.; Naveen, S.; Raghu, A. V. Recent Advances in Layered Clays–Intercalated Polymer Nanohybrids. In *Modified Clay and Zeolite Nanocomposite Materials*; Elsevier, 2019; pp 197–218. <https://doi.org/10.1016/B978-0-12-814617-0.00013-X>.
- [3] Advancing Sustainable Materials Management: 2018 Fact Sheet. 25.
- [4] Franco-Urquiza, E. A. Clay-Based Polymer Nanocomposites: Essential Work of Fracture. *Polymers* **2021**, *13* (15), 2399. <https://doi.org/10.3390/polym13152399>.
- [5] Peng, J.; Yi, H.; Song, S.; Zhan, W.; Zhao, Y. Driving Force for the Swelling of Montmorillonite as Affected by Surface Charge and Exchangeable Cations: A Molecular Dynamic Study. *Results in Physics* **2019**, *12*, 113–117. <https://doi.org/10.1016/j.rinp.2018.11.011>.
- [6] Chiu, C.-W.; Lin, J.-J. Self-Assembly Behavior of Polymer-Assisted Clays. *Progress in Polymer Science* **2012**, *37* (3), 406–444. <https://doi.org/10.1016/j.progpolymsci.2011.07.007>.
- [7] Ou, X.; Lin, Z.; Li, J. Surface Microstructure Engenders Unusual Hydrophobicity in Phyllosilicates. *Chem. Commun.* **2018**, *54* (43), 5418–5421.
- [8] Kubišová, H.; Měřínská, D.; Svoboda, P. PP/Clay Nanocomposite: Optimization of Mixing Conditions with Respect to Mechanical Properties. *Polym. Bull.* **2010**, *65* (5), 533–541.
- [9] Priscila Anadão (2012). Polymer/ Clay Nanocomposites: Concepts, Researches, Applications and Trends for The Future, Nanocomposites - New Trends and Developments. *IntechOpen*. <https://doi.org/10.5772/chapters/37483>.
- [10] Caccamo, M. T.; Mavilia, G.; Mavilia, L.; Lombardo, D.; Magazù, S. Self-Assembly Processes in Hydrated Montmorillonite by FTIR Investigations. *Materials* **2020**, *13* (5), 1100. <https://doi.org/10.3390/ma13051100>.
- [11] Dor, M.; Levi-Kalisman, Y.; Day-Stirrat, R. J.; Mishaël, Y.; Emmanuel, S. Assembly of Clay Mineral Platelets, Tactoids, and Aggregates: Effect of Mineral Structure and Solution Salinity. *Journal of Colloid and Interface Science* **2020**, *566*, 163–170. <https://doi.org/10.1016/j.jcis.2020.01.084>.

- [12] Tarablsi, B.; Delaite, C.; Brendle, J.; Croutxe-Barghorn, C. Maghemite Intercalated Montmorillonite as New Nanofillers for Photopolymers. *Nanomaterials* **2012**, 2 (4), 413–427. <https://doi.org/10.3390/nano2040413>.
- [13] Cygan, R. T.; Greathouse, J. A.; Heinz, H.; Kalinichev, A. G. Molecular Models and Simulations of Layered Materials. *J. Mater. Chem.* **2009**, 19 (17), 2470. <https://doi.org/10.1039/b819076c>.
- [14] Giner, E.; Franco, V.; Vercher, A. Estimation of the Reinforcement Factor for Calculating E2 With The Halpin-Tsai Equations Using The Finite Element Method. **2014**, 8.
- [15] Beall, G. W.; Powell, C. E. *Fundamentals of Polymer-Clay Nanocomposites*; Cambridge University Press: Cambridge ; New York, 2011.
- [16] Wang, J.; Cheng, Q.; Lin, L.; Chen, L.; Jiang, L. Understanding the Relationship of Performance with Nanofiller Content in the Biomimetic Layered Nanocomposites. *Nanoscale* **2013**, 5 (14), 6356. <https://doi.org/10.1039/c3nr00801k>.
- [17] Tehrani, A. H.; Abu Al-Rub, R. K. Mesomechanical Modeling of Polymer/Clay Nanocomposites Using a Viscoelastic-Viscoplastic-Viscodamage Constitutive Model. *Journal of Engineering Materials and Technology* **2011**, 133 (4), 041011. <https://doi.org/10.1115/1.4004696>.
- [18] Jaya Vinse Ruban, Y.; Ginil Mon, S.; Vetha Roy, D. Chemical Resistance/Thermal and Mechanical Properties of Unsaturated Polyester-Based Nanocomposites. *Appl Nanosci* **2014**, 4 (2), 233–240. <https://doi.org/10.1007/s13204-013-0193-1>.
- [19] Wang, Y.-C.; Huang, T.-K.; Tung, S.-H.; Wu, T.-M.; Lin, J.-J. Self-Assembled Clay Films with a Platelet–Void Multilayered Nanostructure and Flame-Blocking Properties. *Sci Rep* **2013**, 3 (1), 2621. <https://doi.org/10.1038/srep02621>.
- [20] Beer, P. D.; Gale, P. A.; Smith, D. K. *Supramolecular Chemistry*; Oxford chemistry primers; Oxford University Press: Oxford ; New York, 1999.
- [21] Kiliaris, P. & Papaspyrides, C. D. Polymer/layered silicate (clay) nanocomposites: An overview of flame retardancy. *Prog. Polym. Sci.* 35, 902–958 (2010).
- [22] Xiong, Z.-Q.; Li, X.-D.; Fu, F.; Li, Y.-N. Performance Evaluation of Laponite as a Mud-Making Material for Drilling Fluids. *Pet. Sci.* **2019**, 16 (4), 890–900. <https://doi.org/10.1007/s12182-018-0298-y>.
- [23] Maiti, M.; Bhowmick, A. K. Synthesis and Properties of New Fluoroelastomer Nanocomposites from Tailored Anionic Layered Magnesium Silicates (Hectorite). *J. Appl. Polym. Sci.* **2008**, 111 (2), 1094–1104. <https://doi.org/10.1002/app.29089>.

- [24] Huang, X.-B.; Sun, J.-S.; Huang, Y.; Yan, B.-C.; Dong, X.-D.; Liu, F.; Wang, R. Laponite: A Promising Nanomaterial to Formulate High-Performance Water-Based Drilling Fluids. *Pet. Sci.* **2021**, *18* (2), 579–590. <https://doi.org/10.1007/s12182-020-00516-z>.
- [25] Arachchige, U. N.; Cruden, A. R.; Weinberg, R. Laponite Gels - Visco-Elasto-Plastic Analogues for Geological Laboratory Modelling. *Tectonophysics* **2021**, *805*, 228773. <https://doi.org/10.1016/j.tecto.2021.228773>.
- [26] Lu, D. R.; Xiao, C. M.; Xu, S. J. Starch-Based Completely Biodegradable Polymer Materials. *Express Polym. Lett.* **2009**, *3* (6), 366–375. <https://doi.org/10.3144/expresspolymlett.2009.46>.
- [27] Svagan, A.; Hedenqvist, M.; Berglund, L. Reduced Water Vapor Sorption in Cellulose Nanocomposites with Starch Matrix. *Composites Science and Technology.* **2009**, *69*, 500-506. <https://doi.org/10.1016/j.compscitech.2008.11.016>.
- [28] Almasi, H.; Ghanbarzadeh, B.; Entezami, A. A. Physicochemical Properties of Starch–CMC–Nanoclay Biodegradable Films. *International Journal of Biological Macromolecules* **2010**, *46* (1), 1–5. <https://doi.org/10.1016/j.ijbiomac.2009.10.001>.
- [29] Huang, M.-Y.; Chen, Y.; Yan, X.; Guo, X.-J.; Dong, L.; Lang, W.-Z. Two-Dimensional Montmorillonite Membranes with Efficient Water Filtration. *Journal of Membrane Science* **2020**, *614*, 118540. <https://doi.org/10.1016/j.memsci.2020.118540>.
- [30] Chanra, J.; Budianto, E.; Soegijono, B. Surface Modification of Montmorillonite by the Use of Organic Cations via Conventional Ion Exchange Method. *IOP Conf. Ser.: Mater. Sci. Eng.* **2019**, *509*, 012057. <https://doi.org/10.1088/1757-899X/509/1/012057>.
- [31] Kim, D.; Mittal, G.; Kim, M.; Kim, S.; Yop Rhee, K. Surface Modification of MMT and Its Effect on Fatigue and Fracture Behavior of Basalt/Epoxy Based Composites in a Seawater Environment. *Applied Surface Science* **2019**, *473*, 55–58. <https://doi.org/10.1016/j.apsusc.2018.12.127>.
- [32] He, H.; Ma, Y.; Zhu, J.; Yuan, P.; Qing, Y. Organoclays Prepared from Montmorillonites with Different Cation Exchange Capacity and Surfactant Configuration. *Applied Clay Science* **2010**, *48* (1–2), 67–72. <https://doi.org/10.1016/j.clay.2009.11.024>.
- [33] Asgari, M.; Abouelmagd, A.; Sundararaj, U. Silane Functionalization of Sodium Montmorillonite Nanoclay and Its Effect on Rheological and Mechanical Properties of HDPE/Clay Nanocomposites. *Applied Clay Science* **2017**, *146*, 439–448. <https://doi.org/10.1016/j.clay.2017.06.035>.

- [34] Malik, N.; Shrivastava, S.; Ghosh, S. B. Moisture Absorption Behaviour of Biopolymer Polycaprolactone (PCL) / Organo Modified Montmorillonite Clay (OMMT) Biocomposite Films. *IOP Conf. Ser.: Mater. Sci. Eng.* **2018**, *346*, 012027. <https://doi.org/10.1088/1757-899X/346/1/012027>.
- [35] Tamaki, R.; Chujo, Y. Synthesis of Poly(Vinyl Alcohol) / Silica Gel Polymer Hybrids by in-Situ Hydrolysis Method. *Appl. Organometal. Chem.* **1998**, *12* (10–11), 755–762. [https://doi.org/10.1002/\(SICI\)1099-0739\(199810/11\)12:10/11<755::AID-AOC783>3.0.CO;2-A](https://doi.org/10.1002/(SICI)1099-0739(199810/11)12:10/11<755::AID-AOC783>3.0.CO;2-A).
- [36] Vasudeo Rane, A.; Kanny, K.; Abitha, V. K.; Patil, S. S.; Thomas, S. Clay–Polymer Composites. In *Clay-Polymer Nanocomposites*; Elsevier, 2017; pp 113–144. <https://doi.org/10.1016/B978-0-323-46153-5.00004-5>.
- [37] Dlamini, D. S.; Mishra, S. B.; Mishra, A. K.; Mamba, B. B. Comparative Studies of the Morphological and Thermal Properties of Clay/Polymer Nanocomposites Synthesized via Melt Blending and Modified Solution Blending Methods. *Journal of Composite Materials* **2011**, *45* (21), 2211–2216. <https://doi.org/10.1177/0021998311401074>.
- [38] Ercan, N.; Durmus, A.; Kaşgöz, A. Comparing of Melt Blending and Solution Mixing Methods on the Physical Properties of Thermoplastic Polyurethane/Organoclay Nanocomposite Films. *Journal of Thermoplastic Composite Materials* **2017**, *30* (7), 950–970. <https://doi.org/10.1177/0892705715614068>.
- [39] Zeng, F.; Xu, X.; Shen, Y.; Liu, Y.; Shan, X.; Qin, Z. Hot–Dog Structured Protective Nanocoating for Multifunctional Cotton Fabrics through Spray–Assisted Layer–by–Layer Assembly. *Cellulose* **2021**, *28* (16), 10637–10654. <https://doi.org/10.1007/s10570-021-04168-z>.
- [40] Cook, R.; Chen, Y.; Beall, G. W. Highly Ordered Self-Assembling Polymer/Clay Nanocomposite Barrier Film. *ACS Appl. Mater. Interfaces* **2015**, *7* (20), 10915–10919. <https://doi.org/10.1021/acsami.5b02162>.
- [41] Graf, D.; Jung, J.; Hanemann, T. Formulation of a Ceramic Ink for 3D Inkjet Printing. *Micromachines* **2021**, *12* (9), 1136. <https://doi.org/10.3390/mi12091136>.
- [42] Mikolajek, M.; Reinheimer, T.; Muth, M.; Hohwieler, P.; Hoffmann, M. J.; Binder, J. R. Control of the Surface Morphology of Ceramic/Polymer Composite Inks for Inkjet Printing. *Adv. Eng. Mater.* **2018**, *20* (9), 1800318. <https://doi.org/10.1002/adem.201800318>.
- [43] Schindelholz, E. J.; Spoerke, E. D.; Nguyen, H.-D.; Grunlan, J. C.; Qin, S.; Bufford, D. C. Extraordinary Corrosion Protection from Polymer–Clay Nanobrick Wall Thin Films. *ACS Appl. Mater. Interfaces* **2018**, *10* (26), 21799–21803. <https://doi.org/10.1021/acsami.8b05865>.

- [44] Priolo, M. A.; Gamboa, D.; Holder, K. M.; Grunlan, J. C. Super Gas Barrier of Transparent Polymer–Clay Multilayer Ultrathin Films. *Nano Lett.* **2010**, *10* (12), 4970–4974. <https://doi.org/10.1021/nl103047k>.
- [45] Tzeng, P.; Maupin, C. R.; Grunlan, J. C. Influence of Polymer Interdiffusion and Clay Concentration on Gas Barrier of Polyelectrolyte/Clay Nanobrick Wall Quadlayer Assemblies. *Journal of Membrane Science* **2014**, *452*, 46–53. <https://doi.org/10.1016/j.memsci.2013.10.039>.
- [46] Adame, D.; Beall, G. Direct Measurement of the Constrained Polymer Region in Polyamide/Clay Nanocomposites and the Implications for Gas Diffusion. *Applied Clay Science* **2009**, *42* (3–4), 545–552. <https://doi.org/10.1016/j.clay.2008.03.005>.
- [47] E.L. Cussler, S.E. Hughes, W.J. Ward Iii, R. Aris, Barrier membranes, *J. Membr. Sci.* **38** (1988) 161–174.
- [48] Derocher, J.; Gettelfinger, B.; Wang, J.; Nuxoll, E.; Cussler, E. Barrier Membranes with Different Sizes of Aligned Flakes. *Journal of Membrane Science* **2005**, *254* (1–2), 21–30. <https://doi.org/10.1016/j.memsci.2004.12.025>.
- [49] Bull, S. J. Nanomechanics of Coatings for Electronic and Optical Applications. *SSP* **2010**, *159*, 11–18. <https://doi.org/10.4028/www.scientific.net/SSP.159.11>.
- [50] Kamal, M. R.; Calderon, J. U.; Lennox, B. R. Surface Energy of Modified Nanoclays and Its Effect on Polymer/Clay Nanocomposites. *Journal of Adhesion Science and Technology* **2009**, *23* (5), 663–688. <https://doi.org/10.1163/156856108X379164>.
- [51] M. Kamal and J. Uribe, ANTEC-SPE Conference Proceedings 64, 357–361 (2006).
- [52] Zhu, J.; Morgan, A. B.; Lamelas, F. J.; Wilkie, C. A. Fire Properties of Polystyrene–Clay Nanocomposites. *Chem. Mater.* **2001**, *13* (10), 3774–3780. <https://doi.org/10.1021/cm000984r>.
- [53] *Impedance Spectroscopy: Theory, Experiment, and Applications*, Third edition.; Barsoukov, E., Macdonald, J. R., Eds.; Wiley: Hoboken, NJ, 2018.
- [54] Percival, S. J.; Melia, M. A.; Alexander, C.; Nelson, D. W.; Spoerke, E. D. Nanoscale Thin Film Corrosion Barriers Enabled by Multilayer Polymer Clay Nanocomposites. 31.
- [55] Macleod, H. A. *Thin-Film Optical Filters*; 2018.
- [56] Nam, H.-J.; Ishii, R.; Ebina, T.; Mizukami, F. Flexible Transparent Self-Standing Binderless Clay Film Prepared by Hydrothermally-Treated Synthetic Clay. *Materials Letters* **2009**, *63* (1), 54–57. <https://doi.org/10.1016/j.matlet.2008.08.057>.

- [57] Barroso, G.; Li, Q.; Bordia, R. K.; Motz, G. Polymeric and Ceramic Silicon-Based Coatings – a Review. *J. Mater. Chem. A* **2019**, 7 (5), 1936–1963. <https://doi.org/10.1039/C8TA09054H>.
- [58] Abed-Elmageed, A. A. I.; Zoromba, M. S.; Hassanien, R.; Al-Hossainy, A. F. Facile Synthesis of Spin-Coated Poly (4-Nitroaniline) Thin Film: Structural and Optical Properties. *Optical Materials* **2020**, 109, 110378. <https://doi.org/10.1016/j.optmat.2020.110378>.
- [59] Ichiki, M.; Lulu Zhang; Zhen Yang; Ikehara, T.; Maeda, R. Thin Film Formation on a Non-Planar Surface by Spray Coating Method. In *Symposium on Design, Test, Integration and Packaging of MEMS/MOEMS 2003*; IEEE: Cannes, France, 2003; pp 300–303. <https://doi.org/10.1109/DTIP.2003.1287057>.
- [60] Mithaiwala, H.; Tronstad, Z. T.; Korah, M. M.; Buffington, A.; Green, M. D. Crosslinked Electrospun Composite Membranes of Poly(Vinyl Alcohol) and Poly(Vinyl Chloride): Tunable Mechanical Properties, Porosity and Performance. *Polym Int* **2021**, 70 (10), 1495–1507. <https://doi.org/10.1002/pi.6224>.
- [61] Zhu X, Cheng X, Luo X, Liu Y, Xu D, Tang X et al., *Environ Sci Technol* 54: 6365–6374 (2020)
- [62] Lamminmäki, T. T.; Kettle, J. P.; Puukko, P. J. T.; Gane, P. A. C. Absorption Capability and Inkjet Ink Colorant Penetration into Binders Commonly Used in Pigmented Paper Coatings. *Ind. Eng. Chem. Res.* **2011**, 50 (6), 3287–3294. <https://doi.org/10.1021/ie102178x>.
- [63] Monne, M. A.; Howlader, C. Q.; Mishra, B.; Chen, M. Y. Synthesis of Printable Polyvinyl Alcohol for Aerosol Jet and Inkjet Printing Technology. *Micromachines* **2021**, 12 (2), 220. <https://doi.org/10.3390/mi12020220>.
- [64] *Emerging Food Packaging Technologies: Principles and Practice*; Yam, K. L., Lee, D. S., Eds.; Woodhead Publishing series in food science, technology and nutrition; Woodhead Pub: Oxford ; Philadelphia, PA, 2012.
- [65] Pandit, S.; Kundu, S. Optical and Structural Behaviors of Crosslinked Polyvinyl Alcohol Thin Films; Mumbai, India, 2018; p 080029. <https://doi.org/10.1063/1.5028863>.